Article

Monitoring Sediment Transport in Certain Harbor Launches in the Southeastern Black Sea

Servet Karasu [1,*], Hasan Oğulcan Marangoz [2], Barbaros Hayrettin Kocapir [2], Enver Yilmaz [3], İsmail Hakkı Özölçer [1] and Adem Akpinar [4]

[1] Department of Civil Engineering, Bülent Ecevit University, Zonguldak 67100, Türkiye; ozolcer@beun.edu.tr
[2] Department of Civil Engineering, Recep Tayyip Erdoğan University, Rize 53100, Türkiye; hasanogulcan.marangoz@erdogan.edu.tr (H.O.M.); bhkocapir@yahoo.com.tr (B.H.K.)
[3] Vocational School of Technical Sciences, Recep Tayyip Erdoğan University, Rize 53100, Türkiye; enver.yilmaz@erdogan.edu.tr
[4] Department of Civil Engineering, Bursa Uludağ University, Bursa 16059, Türkiye; ademakpinar@uludag.edu.tr
* Correspondence: skarasu@beun.edu.tr

Abstract: The problem of shoaling on coastal structures is the result of an event that occurs as part of the natural cycle. In cases where shoaling cannot be detected or prevented, various economic and operational problems may arise and may cause disruptions. In this study, the complex coastal dynamic impact of shoaling on three sequential fishery coastal structures located within the borders of Rize province in the Eastern Black Sea region of Türkiye was examined in terms of bathymetric changes and sediment transport under the influence of the incident wave climate. The effects of these structures on each other were also investigated. With this aim, bathymetric measurements were carried out to examine the impact of waves on seabed erosion and deposition. A serious shoaling problem was identified at one of the harbor launches under investigation, where approximately 13,200 m^3 of deposition occurs annually in a relatively small harbor launch area. Such physical problems are thought to be the result of shoaling, the selection of sites that are not viable for fishery-related coastal structures, or the wrong positioning of the breakwater.

Keywords: shoaling; coastal sedimentation; bathymetric changes; wave impact; fishery harbor

1. Introduction

One of the most important problems faced by structures built on the coast is that of accumulation (sedimentation) or erosion, which occurs because of the disruption of the sediment transport balance. Coastal erosion is a natural process resulting from the dynamic nature of the coastal environment (i.e., the nearshore wave regime and the frequency of storm events), the characteristics of the coastal zone (i.e., the lithology and beach slope), and human impacts (i.e., the removal of coastal ecosystems and the damming of rivers) [1–5]. Even if the shore is in a position of dynamic equilibrium before the construction of the structure, various local erosion or sedimentation problems may occur after the structure has been constructed. The shape, type, size, and extent of the damage caused by these problems are closely related to the wave climate of the region, coastal sediment flow, sediment properties, and the characteristics of coastal structures. The most important sedimentation problem faced by coastal structures that have been built for the development of fishery activities is that the basins of these structures are filled with various solid materials (sediment), such as gravel, sand, and clay. The sediments are transported into the basins, accumulate therein, and cause the basins to become shallower over time, making it difficult, sometimes impossible, for various sizes of boats to berth on these fishery coastal structures. If the structures encounter such shoaling problems, the solutions that will be required to prevent sedimentation will incur some additional costs. Considering that this situation

applies in most fishery coastal structures, significant dredging will be required. Thus, a considerable amount of money will be needed. Before these structures are designed, detailed field studies should be carried out to avoid such problems or to minimize the problems that may occur in the future.

Sedimentation has caused various problems on many coasts around the world. A proper understanding of coastal morphological changes is essential for the integrated management and sustainable development of the coastal zone [6]. Many researchers have tried to examine this problem using different methods and tools. Initially, the main problem was obtaining the bathymetric data since analyzing and interpreting the effect of coastal sedimentation is performed using a high-precision bed surface. Some researchers have focused on creating and then using a surface model via traditional methods [7–16]; however, with the newest survey technology, remote sensing is possible. This technique provides an opportunity to ascertain the seabed morphology with minimum effort. Although remote sensing applications are very common and popular, the various forms have different advantages over each other. In addition, satellite images are sometimes very useful [17–22]. Free-of-charge images are a cheap and affordable way to acquire shallow-water data. Another form of remote sensing technology is LiDAR, which offers high precision but is expensive [23–26]. Employing a photo-based solution using drones (tricopters, quadcopters, hexacopters, etc.) is rarely practical [27].

Previous researchers conducted an experimental study to test the efficiency of the physical model on sediment transport in the nearshore environment [28,29]. Moreover, others tested the results using a numerical model [30–37]. When extra validations are needed, a combined form derived from the various numerical and experimental models can be used to describe the sedimentation problem [38–41].

Based on the bathymetry survey, traditional ways of mapping are more reliable and precise than remote sensing techniques. Traditional bathymetry survey methods typically involve the use of a single-beam or multibeam echo sounder. These methods have been used for many years and are well established, making them reliable for hydrographic surveys. In this study, the shoaling processes seen in some harbor launches (at Sarayköy, Sandıktaş, and Yanıktaş in Rize, Türkiye) were monitored in the traditional manner (Figure 1). Accordingly, this study was conducted to determine the compatibility and consistency of the surface model obtained through bathymetry and shallow-water surveys carried out periodically, along with the sieve analysis of the sediment samples taken from the same place in each survey period, and the results were compared to existing maps to identify changes in bathymetry. Field studies were carried out to determine the bathymetric changes and monitor any specific scenario by focusing on a particular structure. Thus, in this study, wave–sediment transport interaction was investigated in three sequential fishery harbors. All bathymetric variations were evaluated based on the wave data and granulometry of the sediment samples. Granulometric variations in the sample points gave hints as to where the sediment came from.

1.1. Distribution of Fishery Coastal Structures in Türkiye

The total length of the Turkish coast is 8483 km, including the Black Sea (1719 km), Marmara (1474 km), and the Mediterranean (2025 km) and Aegean (3265 km) coastal regions [42]. There are 358 fishery coastal structures in operation along the entire Turkish coast (including the undefined structures) (Table 1). A fishery harbor (FH) is a place where fishing boats can be tied up, while a harbor launch (HL) is a slipway where boats, barges, and small ships are pulled ashore. Every one of the harbor launches and fishery harbors are described as fishery coastal structures (FCSs). There is a total of 98 FCSs in the provinces of Artvin, Rize, Trabzon, and Giresun in the Eastern Black Sea region [43]. The types of these structures and their distribution are given according to their provinces in Table 2. Rize province has a coastline of 80 km. It has a total of 39 fishery coastal structures, including 5 fishery harbors and 34 harbor launches. Rize province has the greatest number of coastal structures in the Eastern Black Sea region, with a proportion of 39.8%.
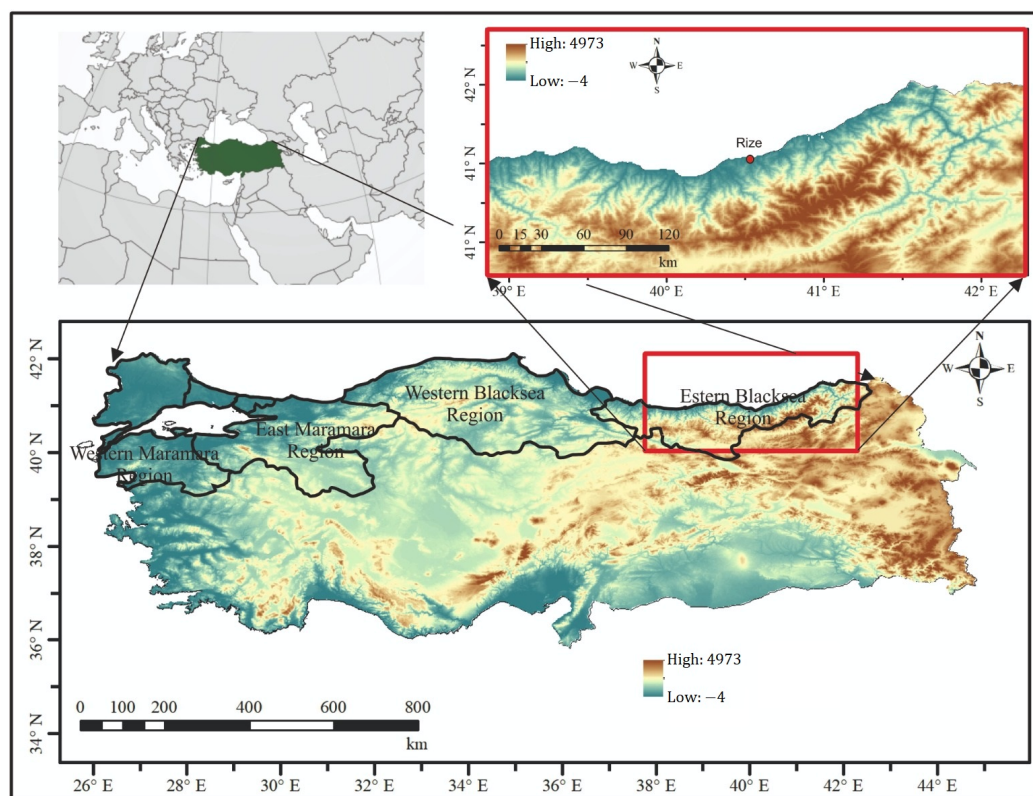
Figure 1. Location maps of Türkiye (**upper left**), the Black Sea regions (**lower image**), and the Eastern Black Sea, showing the location of Rize (**upper right**).

Table 1. Distribution of fishery coastal structures (FCSs), grouped according to region [43]. "Other" includes natural shelters, berthing places, and piers.

Region	Fishery Harbor (FH)	Harbor Launch (HL)	Other	Total
Eastern and Middle Black Sea	40	83	2	125
Western Black Sea	29	12	3	44
Marmara	66	18	1	85
Aegean	60	22	3	85
Mediterranean	16	1	2	19
Internal Water	3	0	2	5

Table 2. Types of fishery coastal structures and their distribution in the Eastern Black Sea region [43].

Province	Coastline Length (km)	Fishery Harbor (FH)	Harbor Launch (HL)	Total	%
Artvin	34	3	5	8	8.2
Rize	80	5	34	39	39.8
Trabzon	135	11	16	27	27.5
Giresun	112	4	20	24	24.5
Total	361	23	75	98	100

1.2. Shoaling Problems on the Turkish Coast

The Eastern Black Sea region has the greatest number of coastal structures in Türkiye. Therefore, fishery coastal structures are of great value for the Eastern Black Sea region. Fishermen are warned to take greater care in the Eastern Black Sea, where fishing is a critical income source for the native population [44]. The occurrence of shoaling in harbor launches is a serious problem since fishing boats cannot maneuver easily in the

extremely shallow waters that result. Some fishery harbors and harbor launches, especially in the Mediterranean and Aegean regions, serve the tourism and transportation sectors as well as the agriculture sector, while most of the coastal structures serve the agricultural sector [43]. Fishery coastal structures that are in need of dredging, according to the Ministry of Transport and Infrastructure's regional directorates, are given in Table 3. As shown in Table 3, 169 (46.6%) of the 363 fishery coastal structures in Türkiye are located in the Black Sea region, with 85 (23.4%) in the Marmara region, 85 (23.4%) in the Aegean region, and 19 (5.2%) in the Mediterranean region. Most of the fishery coastal structures (55.1%) in these regions require dredging. The Black Sea region demonstrates the greatest need for dredging, with 78 FCSs. Fishery coastal structures that are in need of dredging in the Eastern Black Sea region are detailed in Table 4. As can be seen, 50 out of the 98 fishery coastal structures within the boundaries of the Eastern Black Sea region require dredging [45].

Table 3. Distribution of fishery coastal structures in need of dredging in Türkiye, grouped according to region [43].

Region	FCSs	FCS/Total FCSs (%)	ND	ND/FCSs (%)	ND/Total FCSs (%)
Black Sea	169	46.6	78	46.2	21.5
Marmara	85	23.4	69	80.3	19.0
Aegean	85	23.4	37	43.5	10.2
Mediterranean	19	5.2	16	84.2	4.4
Internal Water	5	1.4			
Total	363		200		55.1

Note: FCS—fishery coastal structure, ND—needs dredging.

Table 4. Distribution of fishery coastal structures in need of dredging in the Eastern Black Sea region, grouped according to province [45].

Province	FCSs	ND	ND/FCSs (%)
Artvin	8	2	25
Rize	39	17	43.6
Trabzon	27	16	59.3
Giresun	24	15	62.5
Total	98	50	

One of the biggest problems faced by fishery harbors is the shoaling of the entrance and the basin of the structure. After this occurs, dredging is inevitable if the basin or inlet of the fishing coastal structure is to continue its operations. Thus, fishing activities will be interrupted. Various studies have been carried out in many parts of the world, exploring ways to avoid or minimize the shoaling problem [6,30,31,35,40]. Of these previous studies, no comprehensive study was found that included fishery harbors and their vicinity, incorporating a detailed bathymetric survey, sediment samples, and an examination of wave properties. The results of this study are of critical importance in terms of making the right decisions during the design phase of fishery coastal structures that are planned to be built in the future. Thus, this study aims to investigate the shoaling mechanism and the source and possible path of sediment transport, causing the accumulation of deposits in three harbor launches of the Eastern Black Sea region that are exposed to severe shoaling. Shallow-water surveys were first carried out periodically in three selected harbor launch areas. Secondly, closure depths were determined, along with sequential profile changes for each study area, and then the study areas were separately divided into sub-regions for evaluation of the erosion or accumulation rates in the harbor launches. Bathymetric surveys and wave parameters were analyzed at certain time intervals, and sediment samples were acquired at several locations. The results obtained from the field studies were examined by evaluating possible reasons for the shoaling problem and, thus, serve to improve our understanding of the physical mechanisms of shoaling around the harbor launches.

2. Study Area

The Eastern Black Sea region has the highest number of fishery coastal structures in Türkiye. Of the 98 fishery coastal structures, 39 (39.8%) in the region are in Rize province. In total, 17 of these fishery coastal structures, almost half of them, need dredging during certain periods. The distribution of the fishery coastal structures that are in need of maintenance, expansion, repair, and dredging in the Eastern Black Sea region, grouped according to province, is shown in Table 5. Based on this information, 10 of the FCSs in Rize province need dredging in the short term and 7 in the medium term. Since the highest number of FCSs requiring dredging are located in Rize, this region is the focus of the current study. While choosing the fishery coastal structures to be investigated, attention was paid to the fact that they were close to each other in terms of location, they were set at different angles (to observe the efficiency of the various coastal structures under the same wave attack), and the volume of shoaling was different. The closeness of the selected coastal structures to each other will enable several observations (wave height, period, and direction) on these structures. The shoaling problems identified by the fishermen in the selected fishery coastal structures were also taken into consideration in their selection. Considering all these parameters, three fishery coastal structures were selected in the Derepazarı and İyidere districts, which are located within the borders of Rize province in the Eastern Black Sea region. The study area and the selected harbor launches are shown in Figure 2.

The short-, medium- and long-term investment program proposals of three FCSs were selected since they fell within the scope of this study, for which the proposed maintenance, dredging, extension (addition), and priority degrees of fishery coastal structures are shown in Table 6. According to this table, it is evident that Sarayköy harbor launch needs repair, dredging, and extension in the medium term, Sandıktaş harbor launch needs dredging in the short term and extension in the long term, and Yanıktaş harbor launch needs dredging and extension in the medium term. The characteristics of the three selected fishery coastal structures are given in Table 7. Sarayköy harbor launch has a main breakwater of 167 m in length, with a secondary breakwater of 80 m in length, and can accommodate 10 fishing boats. The distance to the city center is 13 km. The length of the main breakwater of the Sandıktaş harbor launch is 290 m, that of the secondary breakwater is 60 m, and it can accommodate 20 fishing boats. The distance to the city center is 10.8 km. Derepazarı Yanıktaş fishery harbor launch has a single breakwater, which is 150 m in length, and can accommodate up to 22 boats.

Table 5. Provincial distribution of fishery coastal structures in need of maintenance, dredging, or additional structures in any term [43], e.g., in Rize, 7 harbor launches need dredging in the medium term.

Provinces with FCS	Short Term			Medium Term			Long Term		
	Maintenance	Dredging	Additional Structures	Maintenance	Dredging	Additional Structures	Maintenance	Dredging	Additional Structures
Artvin	2	-	1	-	2	3	-	-	-
Rize	5	10	14	2	7	8	-	-	-
Trabzon	2	3	3	-	1	2	1	1	1
Giresun	-	-	-	-	-	-	-	-	-

Figure 2. General view of selected harbor launches in Rize province: Sarayköy, Sandıktaş, and Yanıktaş.

Table 6. Proposed repair, dredging, extension, and prioritization of fishery coastal structures (3 selected harbor launches) [43].

Name	Class	District	Short Term			Medium Term			Long Term		
			Maintenance	Dredging	Extension	Maintenance	Dredging	Extension	Maintenance	Dredging	Extension
Sarayköy	Harbor Launch	İyidere	-	-	-	Yes	Yes	Yes	-	-	-
Sandıktaş	Harbor Launch	Derepazarı	-	Yes	-	-	-	-	-	-	Yes
Yanıktaş	Harbor Launch	Derepazarı	-	-	-	-	Yes	Yes	-	-	-

Table 7. Some specifications of the harbor launches of interest.

	Sarayköy Harbor Launch	Sandıktaş Harbor Launch	Yanıktaş Harbor Launch
Category	Under operation	Under operation	Under operation
Main breakwater length (m)	167	290	150
Secondary breakwater length (m)	80	60	0
Pier capacity	0	0	0
Boat capacity	10	20	22
The angle of the main breakwater with respect to north (in degrees)	55	100	90

3. Materials and Methods

3.1. Field Surveys

Field studies are extremely important for the planning, protection, and operation of coastal structures, which make significant economic contributions to the region. A series of field studies was carried out to monitor the shoaling processes of the FCSs, specifically, the source and path of sediment transport, which affects the shoaling. Field surveys were conducted in two areas, one at sea and one on the land, to monitor sediment transport in the vicinity of fishery coastal structures. Initially, we planned to observe seabed changes by conducting a total of three bathymetric surveys (summer–winter–summer), performed once every 6 months. However, the fact that the weather and wave conditions in the sea were not always suitable caused the planned survey periods to change. Therefore, surveys were carried out on the dates specified in Table 8.

Table 8. Surveying dates of the Sandıktaş, Yanıktaş, and Sarayköy harbor launches.

Called ID	Dates	Harbor Launch
s_1	2 June 2016	Sarayköy
y_1	20 June 2016	Yanıktaş
s_2	29 April 2017	Sarayköy
n_1/y_2	7 February 2017	Sandıktaş/Yanıktaş
s_3	4 November 2017	Sarayköy
n_2/y_3	5 November 2017	Sandıktaş/Yanıktaş
n_3	8 April 2018	Sandıktaş

In bathymetric surveys, the boat, which is equipped with various instruments, may not be able to access and measure the depths in shallow water. Therefore, the shallow-water measurements were taken manually. Unlike in the sea measurements, the surveys were conducted more often in those parts where the slope changes frequently or abruptly and were less frequent in the regions with flat and constant slopes. A Topcon HiPer V rover (multidirectional GNSS receiver) was used for the shallow-water surveys, and CORS-TR was used as the measurement system. The height correction of the satellite receiver was made according to a reference point with a certain elevation. This correction was repeated for each survey. The most important step in generating bathymetric maps is the comprehensive and reliable sensing of the seabed's topography. The boat to be operated when taking the measurements should proceed at a speed of approximately 4 knots and have sufficient maneuverability. Therefore, a rubber boat of 3 m in length was used for the sea measurements. Due to the stability and safe driving conditions provided by the boat, the predetermined measurement lines could be followed as accurately as possible. The boat was equipped with the following instruments: a Topcon HiPer V mobile satellite receiver, an Ohmex SonarMite-BTX single-beam echo sounder, an AML Oceanographic BASE X device (which is used to measure the propagation speed of sound in water to ensure high precision in the measurements), and a computer (which is used for the synchronous recording of navigation, depth, and spatial data). Using an echo-sounder, measurements were taken to 10 m in depth with high resolution (accuracy at the centimeter level). With the help of the smart transducer and the bottom-tracking feature, the depths were digitally recorded on the computer with the quality note. The data being received from both the echo-sounder and the SonarMite were simultaneously recorded independently through a timestamp with 1-millisecond precision. Simultaneous position data were collected using the Kordil Navigation Pro software (v2). Depths were converted to the TUDKA (Turkish National Vertical Control Network) system, regardless of the sea level that was measured, while considering the water level changes being recorded simultaneously with bathymetric measurements. Surveying line spacing that was wider than 15 m was not allowed in the measurements, to ensure that the bathymetry changes can be examined with reasonable accuracy (Figures 3 and 4). The preprepared lines of the first survey were tracked for the following surveys. The survey lines were followed using a PC screen on the boat. This

procedure ensured that the point iterations of the sea surveys were performed from nearly the same points.
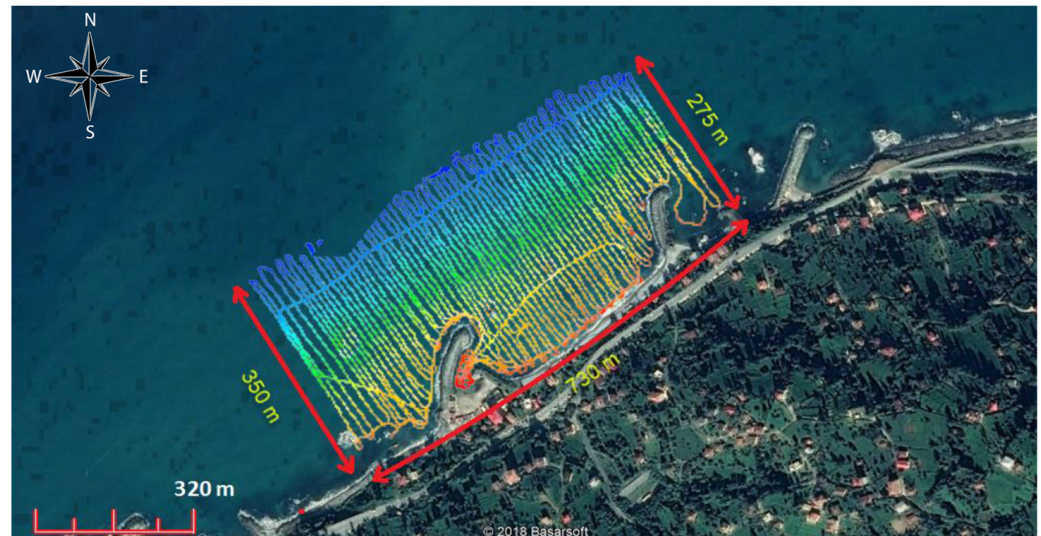
Figure 3. Survey lines for the İyidere Sarayköy harbor launch.
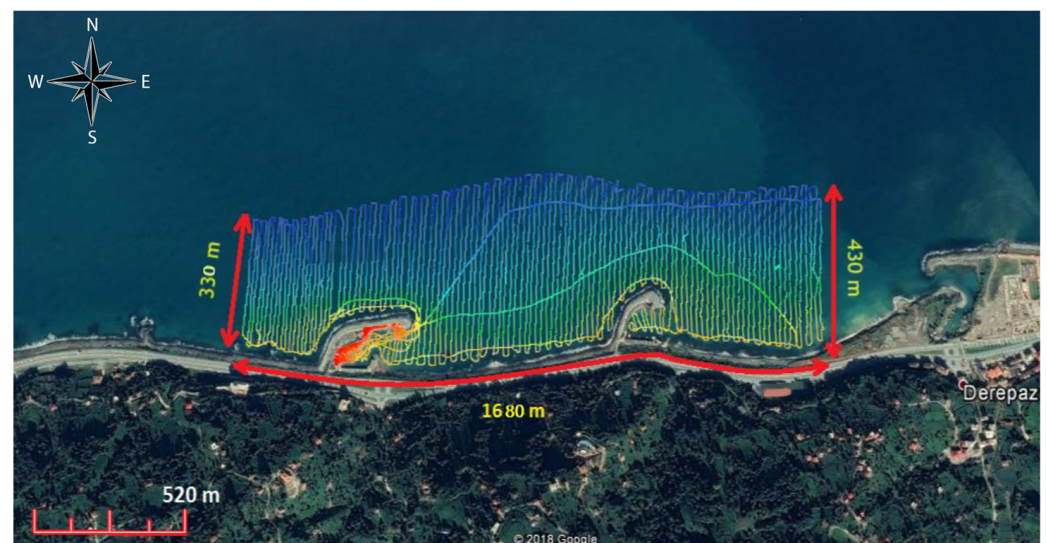
Figure 4. Survey lines for the Sandıktaş and Yanıktaş harbor launches.

Positioning was performed using the Topcon HiPer V mobile GNSS (Global Navigation Satellite System) instrument using the CORS system. The CORS system consists of fixed observation stations, which are used by many countries and are in certain locations at set intervals to present the spatial coordinates of a particular point to the user, with the necessary corrections being made precisely [46]. With the CORS-TR system, the mobile receiver was positioned on the boat for the sea surveys and on a life jacket for shallow-water surveys. The raw data of the GPS antenna were recorded simultaneously. To confirm whether the initial and final readings were linear or not, the NMEA (American National Marine Electronics Association) GGA message, recorded with the Kordil Navigation Pro software and the RTK antenna elevations extracted from this message, was used.

It was necessary to correct the depth values using sound velocity propagation. Hence, the AML Oceanographic BASE-X instrument, which determines the sound velocities in the sea by using properties of the temperature and salinity properties of water, was used in the measurements. According to the density of the aquatic environment, sound velocity

propagation (SVP) ranges from 1390 to 1650 m/s. SVP on the water surface, measured at 15 °C and 3.2% salinity, was 1500 m/s. SVP in the sea can be between 1470 and 1500 m/s, on average. The general relation of SVP is calculated as follows:

$$SVP = 1449.2 + 4.6t - (0.055t^2) + (0.00029t^3) + (1.34 - 0.01t)(s - 35) + 0.016d \qquad (1)$$

where SVP is the propagation velocity of sound in water (m/s), t represents the water temperature (°C), d is the depth from the sea surface (m), and s is the salinity of the water ($^0/_{00}$).

The root mean square error (RMSE) method was used to check the reliability of measurements in the region where there was no sediment transport. The RMSE value was found to be 0.03 m, which shows that the measurement reliability is quite high in the selected regions.

$$RMSE = \sqrt{\frac{\sum_{i=1}^{n} (e_i)^2}{n}} \qquad (2)$$

Here, e_i is the depth for any survey point, while n is the data number.

During data processing, Kordil Geodesy Tools + SonarMagic and PDS2000 software (v.3.9.2.5) were used. The data collected through the time label were combined with the Kordil Sonar Magic software (v.2.6.1) and then corrected using the SVP, offset, and water level heights. Coordinates with the date and time data were transferred to the PDS2000 program. The profiles were examined and unrealistic data were discarded. Finally, the edited profiles were mapped in the PDS2000 plot module.

3.2. Sea Level Measurement

Sea level measurements were taken before and after the surveys. If there were differences larger than 2–3 cm, this difference was evaluated in the data analysis by considering the readings on the instrument elevation during bathymetry measurements. The sea level was measured from a polygon point on a pier located near the study area, just before and after the bathymetry surveys. The actual depth value was determined by correcting the measured sea level, as in the formula given below:

$$RL = (SL - TD)(SVP/1500) \qquad (3)$$

where RL represents the real level, SL represents sea level, TD represents the transducer draft, and SVP represents the propagation speed of a sound wave in the sea (m/s).

It is known that the average water level change interval in the Black Sea is small. The authors of [47] reported that the difference between the monthly mean highest and lowest sea level was 19 cm, while the authors of [48] reported that the mean seasonal sea level anomalies of the Black Sea were 20 cm. The author of [49] stated that the tidal amplitudes in the Black Sea were very small (3–9 cm) compared to other seas in the world. Every sea survey took 5–6 h. Thus, bathymetric data were not affected by sea level changes during the survey period.

3.3. Sediment Properties of the Fields

Sediment samples were taken from various depths in each region to represent the upstream, downstream, and inner (basin) and outer parts of the harbor launch. The sampling points of the Sandıktaş, Yanıktaş, and Sarayköy HLs are shown in Figures 5 and 6, respectively. A sieve analysis test was carried out to determine the particle size distribution of the samples, for which 0.5–1.0 kg samples were taken. The sieve analysis test was carried out according to the methods specified for the standard given in [50], and sieves with the sieve mesh diameter specified in this standard were used in the tests. No organic matter was observed in the samples that were taken. By using the obtained data, the particle size distribution (granulometry) curves of the sediment samples were obtained. The d_{30} and d_{60} and the effective grain size (d_{10}) on the sieve analysis curve were obtained, and

the values of the coefficient of uniformity ($Cu = d_{60}/d_{10}$) and the gradation coefficient ($Cc = (d_{30})^2/(d_{10}.d_{60})$) were calculated. Sediment samples were classified by using Cu and Cc values. The unified soil classification system (USCS) method was used when classifying the soil samples. While making this classification, the standards recommended in [51] were used. In this system, the soil class was determined by using the passing percentages of the 200-micron and 4 mm sieves and the Cu and Cc values. As a result of these evaluations, it was determined that the sediment samples taken from the Sandıktaş and Yanıktaş regions were in the SP (poorly graded sand) and SC–SM (clay sand–silty sand) class, while the samples from the Sarayköy region were in the SP (poorly graded sand) class (Tables 9 and 10). The average grain size ($D_{50} = 0.37$ mm) was closely similar inside, upstream, and downstream of the breakwater. From the coast to the offshore region, the average grain diameter decreased gradually.
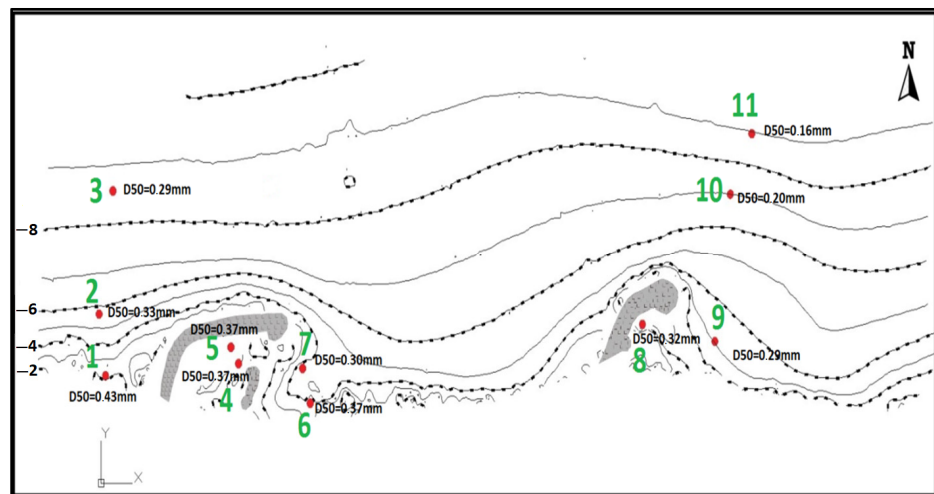
Figure 5. The points from which the sediment samples were taken at the Sandıktaş and Yanıktaş HLs.
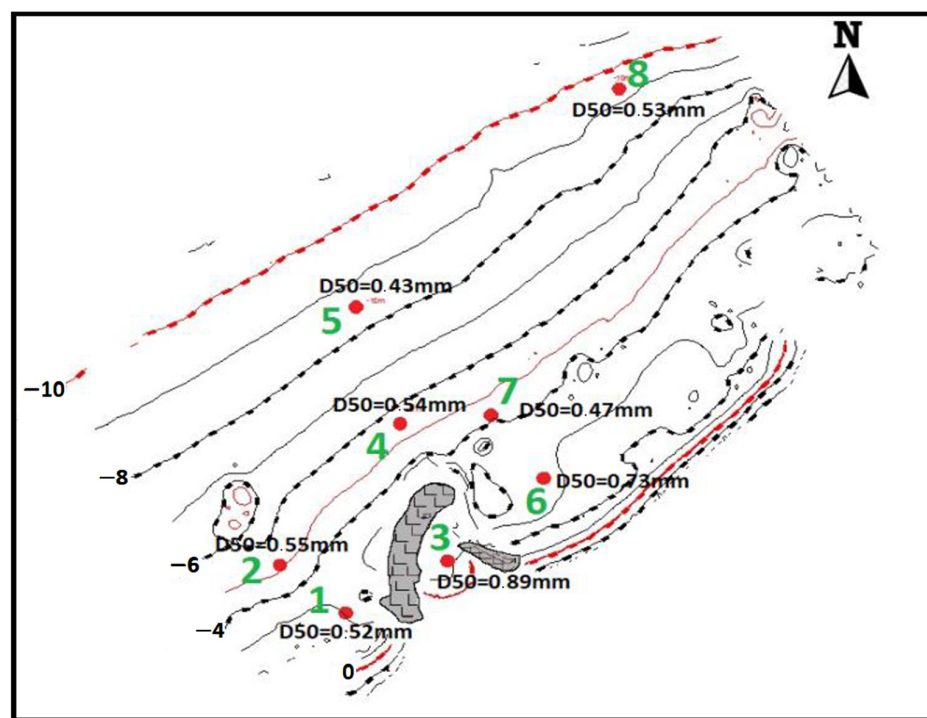
Figure 6. The points from which the sediment samples were taken at Sarayköy HL.

Table 9. Evaluation of sediment samples according to the USCS soil classification system, sampled from the Sandıktaş and Yanıktaş HLs.

Number of Samples	Sample Weight (g)	Remaining in Sieve No. 200	Remaining in Sieve No. 4	d_{10} (mm)	d_{30} (mm)	d_{50} (mm)	d_{60} (mm)	C_u	C_c	USCS Soil Class
1	492	100	0	0.27	0.34	0.43	0.50	1.85	0.87	SP
2	456	98.2	0	0.16	0.27	0.33	0.36	2.30	1.34	SP
3	484	95.5	0	0.12	0.20	0.29	0.32	2.67	1.03	SP
4	776	99.5	0	0.21	0.30	0.37	0.41	1.93	1.03	SP
5	942	99.6	0	0.16	0.29	0.37	0.42	2.54	1.20	SP
6	998	99.8	0	0.21	0.30	0.37	0.41	1.92	1.03	SP
7	314	99.4	0	0.14	0.25	0.30	0.32	2.27	1.41	SP
8	928	100	0	0.22	0.28	0.32	0.34	1.56	1.06	SP
9	416	99.5	0	0.14	0.23	0.29	0.32	2.34	1.24	SP
10	292	95.2	0	0.11	0.15	0.20	0.23	2.05	0.87	SP
11	162	90.1	0	0.11	0.13	0.16	0.18	1.72	0.90	SC/SM

Table 10. Evaluation of the sediment samples according to the USCS soil classification system, sampled from Sarayköy HL.

Number of Samples	Sample Weight (g)	Remaining in Sieve No. 200	Remaining in Sieve No. 4	d_{10} (mm)	d_{30} (mm)	d_{50} (mm)	d_{60} (mm)	C_u	C_c	USCS Soil Class
1	554	99.6	0	0.28	0.43	0.52	0.58	2.07	1.14	SP
2	346	99.4	0	0.28	0.46	0.55	0.60	2.11	1.23	SP
3	396	100	0	0.45	0.66	0.89	0.96	2.13	1.01	SP
4	308	100	0	0.28	0.45	0.54	0.60	2.13	1.19	SP
5	40	100	0	0.15	0.28	0.43	0.50	3.32	1.04	SP
6	300	100	0	0.45	0.57	0.73	0.83	1.86	0.88	SP
7	236	100	0	0.23	0.34	0.47	0.53	2.29	0.97	SP
8	142	100	0	0.25	0.43	0.53	0.59	2.35	1.23	SP

3.4. Determination of Off-Shore Wave Conditions in the Study Area

To determine the wave conditions, the third-generation spectral wave hindcast model, SWAN Cycle III version 41.01, developed by [52,53] was applied. The model was adapted to the Black Sea, as suggested by the authors of [54]. The first of the two-input datasets required by the wave hindcast model was the general bathymetric charts of the ocean (GEBCO) bathymetry data [55], which covers the entire Black Sea with a spatial resolution of 30 arc seconds, and the second is the climate forecast system reanalysis (CFSR) wind fields dataset [56]. The CFSR winds have a temporal resolution of 1 h and a spatial resolution of $0.2045° \times 0.2045°$. For SWAN simulations, a uniform (homogeneous), rectangular (regular) computational area was defined, covering an area of approximately 1170 km by 880 km, including the entire Black Sea. This area covers approximately 8° latitude (40° N–48° N) and 15° longitude (27° E–42° E). The numerical resolution is constrained by 226 and 121 digital mesh points in the *x* and *y* directions of the geographic area, respectively, and was created as equal to approximately $0.067° \times 0.067°$. The spectral field was divided into 24 equal directions in a 360° cycle, and the calculations were performed at 30 logarithmic frequencies between 0.04 Hz and 1.0 Hz. For the output of the model results, the temporal resolution was set to 30 min, and the SWAN model was applied in the third-generation and nonstationary mode. In the model, since the Black Sea is almost enclosed, the boundary condition was not used, and the currents were not examined.

Most of the physical adjustments for the wave model calculations were based on the default adjustments of the SWAN model. However, different settings were preferred in this study for the wind input and whitecapping processes. Ref. [54] examined how the performance of the model would change as a result of the combinations created between different wind input and whitecapping formulations and when the different whitecapping coefficients that were used presented an optimum adjustment for the Black Sea. The physical adjustments recommended by the authors of [54] were used in this study. Accordingly,

for the wind input process, the formulations from [57] and those from [58,59] were used for the whitecapping process, and the whitecapping coefficient was set to 1.5. Using the values of $\lambda = 0.25$ and $C_{nl4} = 3 \times 10^7$ for the quadruplet wave interactions, the discrete interaction approach used in Ref. [60] was employed. The JONSWAP friction formulation of $C_{fjon} = 0.038$ m^2 s^{-3} was used, which was based on that used by the authors of [61]. Depth-induced wave breaking was modeled according to the approach taken in [62], using the values of $\alpha = 1$ and $\gamma = 0.73$. Three-wave interactions were activated based on the approach adopted by the authors of [63]. Thus, a spectral wave modeling technique including both offshore (wind wave growth, whitecapping, and quadruplet wave interactions) and nearshore (bottom friction, wave breaking, and triad wave interactions) physical processes were performed for the period from 1 June 2016 to 8 April 2018, and all the desired wind and wave parameters were accumulated for this time interval at all the chosen locations.

Since the main focus of this study was on those regions where the relevant fishery coastal structures (FCSs) are located (Figure 2), approximately eight stations were chosen that were located offshore from the harbor launches to represent the wind and wave conditions of each sub-region from west to east. The simulation results were examined, and it was determined that all stations showed a similar feature for each sub-region. For this reason, the results for a selected station in each sub-region were analyzed separately for each year within the 2016–2018 period.

4. Results and Discussion

This section presents the shallow-water surveys and details of the examined areas in the sub-regions and evaluates the bathymetric changes in the harbor launches based on bathymetry difference maps, average water depths, and wave conditions.

4.1. Shallow-Water Surveys

Shallow-water surveys were carried out periodically in three selected harbor launch areas. The measurement areas were determined to be sufficiently large to observe not only the shoaling of the basin in which these structures are located but also the possible path of sediment transport. After the surveys, all data were processed, and the bathymetry maps that were obtained from studies conducted for three different regions are shown below (Figure 7). For each harbor launch, the first survey was taken as a reference, then the depth-difference maps were created by either subtracting from each bathymetry value or adding to each one.

4.2. Determining the Examined Areas

The bathymetric variation around any coastal structure cannot be the same in all locations; in some areas, erosion may occur, while in others, deposition may be more dominant. Therefore, the study areas were divided into certain sub-regions, evaluating the conditions separately for the harbor launches. The area in the vicinity of the Yanıktaş harbor launch was divided into four regions for evaluation. Accordingly, region C represents the basin, region A represents the updrift, region D represents the downdrift of the harbor launch, and region B represents the upper part of the breakwater. The regions are shown in Figure 8, based on the difference map created between the second and third surveys. Two profiles, SEC-350 and SEC-750, are shown in Figure 9. From these profiles, it was observed that the bed changes were negligibly low at depths deeper than −7 m. The northern border line of the regions created for all the selected harbor launches was determined to be between −6 m and −7 m in depth, and areas deeper than those measured within this border were not included in the evaluations.
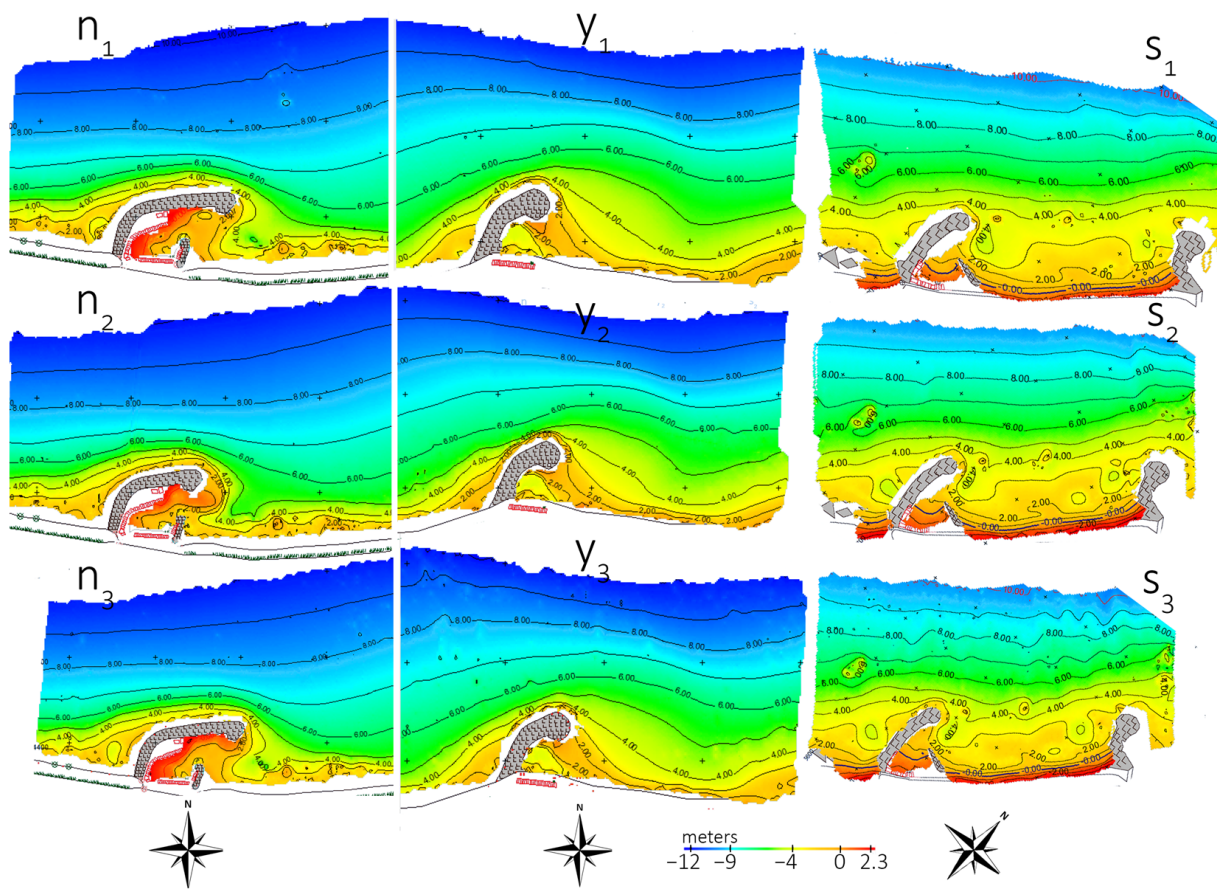
Figure 7. Bathymetry of Sandıktaş, Yanıktaş, and Sarayköy HLs on the surveying dates (the $n_{1,2,3}$, $y_{1,2,3}$, and $s_{1,2,3}$ indexes represent the caller identities of Sandıktaş HL, Yanıktaş HL, and Sarayköy HL, respectively).
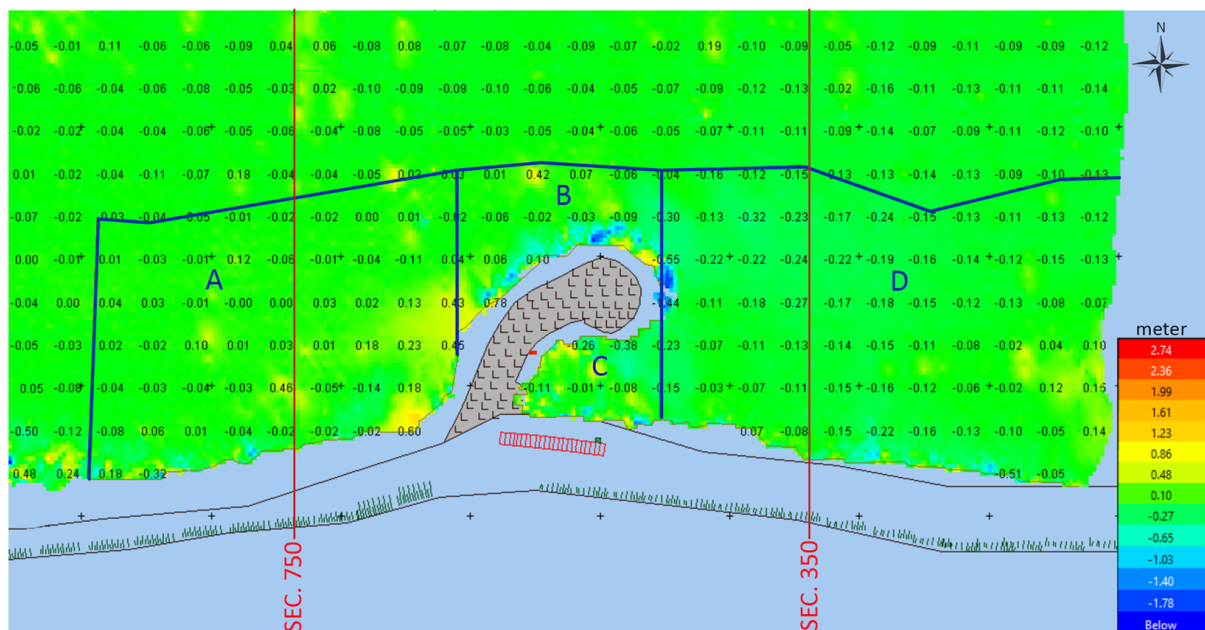
Figure 8. The determined regions for the Yanıktaş HL and the plan view of the cross-section. Regions C, A, and D represent the basin, updrift, and downdrift of the harbor launch, respectively, while region B represents the upper part of the breakwater (negative value refers to the erosion, while positive value refers to the accretion between second and third surveys).
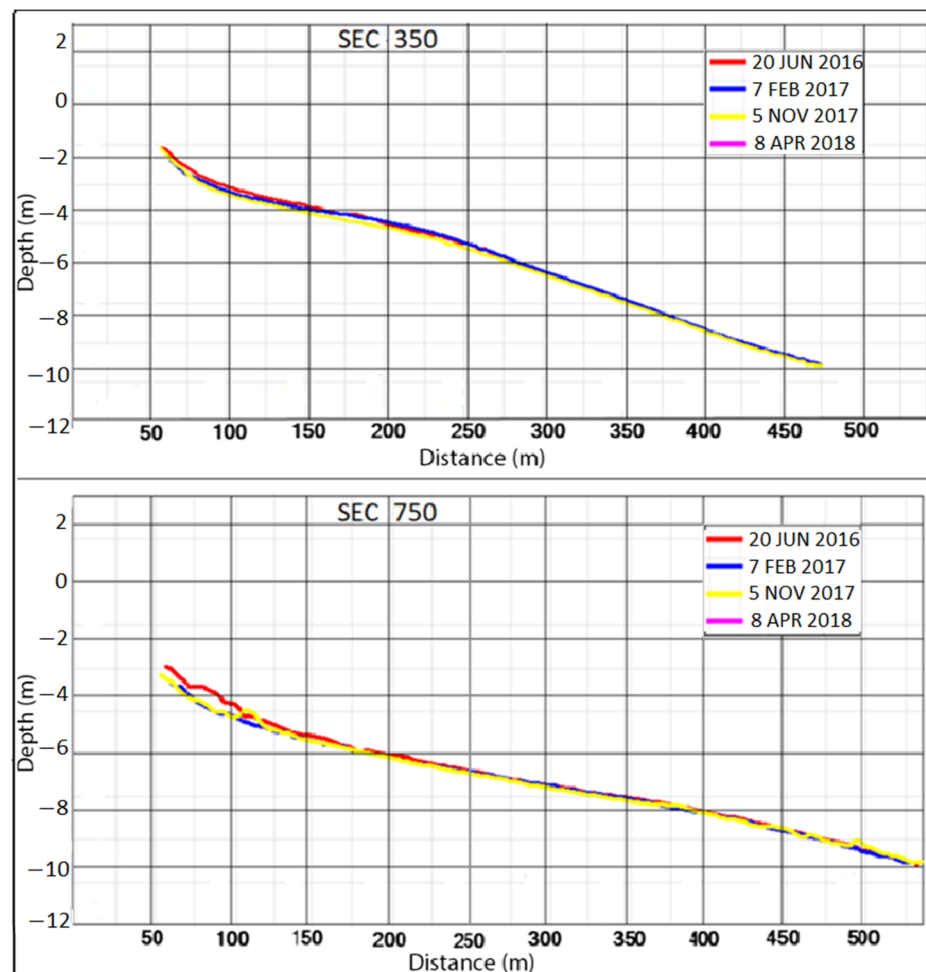
Figure 9. The sequential profile changes recorded for the Yanıktaş HL.

The line was drawn vertically from the starting point of the main breakwater to the northern boundary line for the Sandıktaş HL. Similarly, vertical lines were drawn from the main breakwater and the shoreline in the downstream region of the breakwater to the northern borderline. The location of the vertical line drawn from the shore downstream of the main breakwater to the northern boundary line was chosen by considering the impact area of the sediment transport. A line parallel to the shore was drawn from the side of the main breakwater to the downstream boundary line. The boundaries of all regions were determined using the lines formed by combining the main breakwater and the secondary breakwater (Figure 10). The profile sections numbered 1150 and 1500 for the Sandıktaş harbor launch are shown in Figure 11. Hence, it was observed that the changes in the seabed were negligibly deeper than −6 m and −7 m.

In Sarayköy's fishery harbor, five separate areas were created and then evaluated independently. Region A represents the area southwest of the breakwater, region D represents the area east of the breakwater, region C represents the area within the harbor, region B represents the western area, and, finally, region E represents the area outside of the breakwater. Here, a vertical line was drawn between regions A and B from the starting point of the main breakwater to a depth where there was no sediment transport. The locations of the vertical lines drawn upstream and downstream of the main breakwater were decided by considering the impact area of the sediment deposition (Figure 12). It is necessary to make evaluations and comparisons in the context of exposure and shoaling. Hence, the angles of the second part of the main breakwaters with an offshore dominant wave direction were determined, to examine the effects of the positioning of the breakwater.
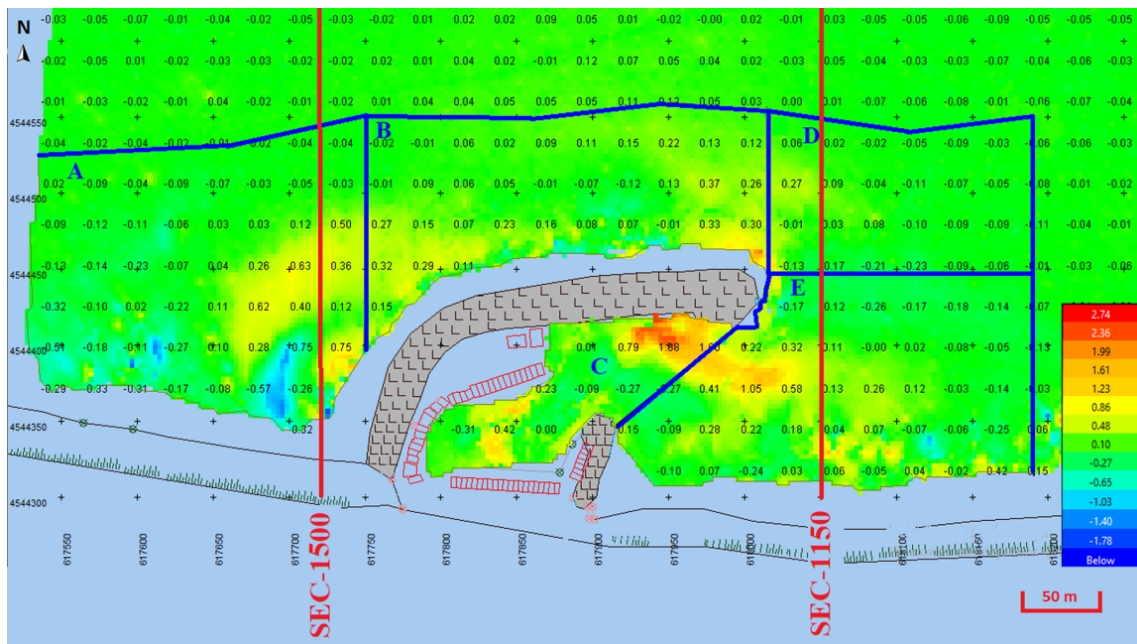
Figure 10. The determined areas for the Sandıktaş HL and a plan view of the cross-sections. Regions C, A, and D represent the basin, updrift, and downdrift of the harbor launch, respectively, while region B and E represent the upper part and eastward of the breakwater, respectively. (negative value refers to the erosion, while positive value refers to the accretion between second and third surveys).
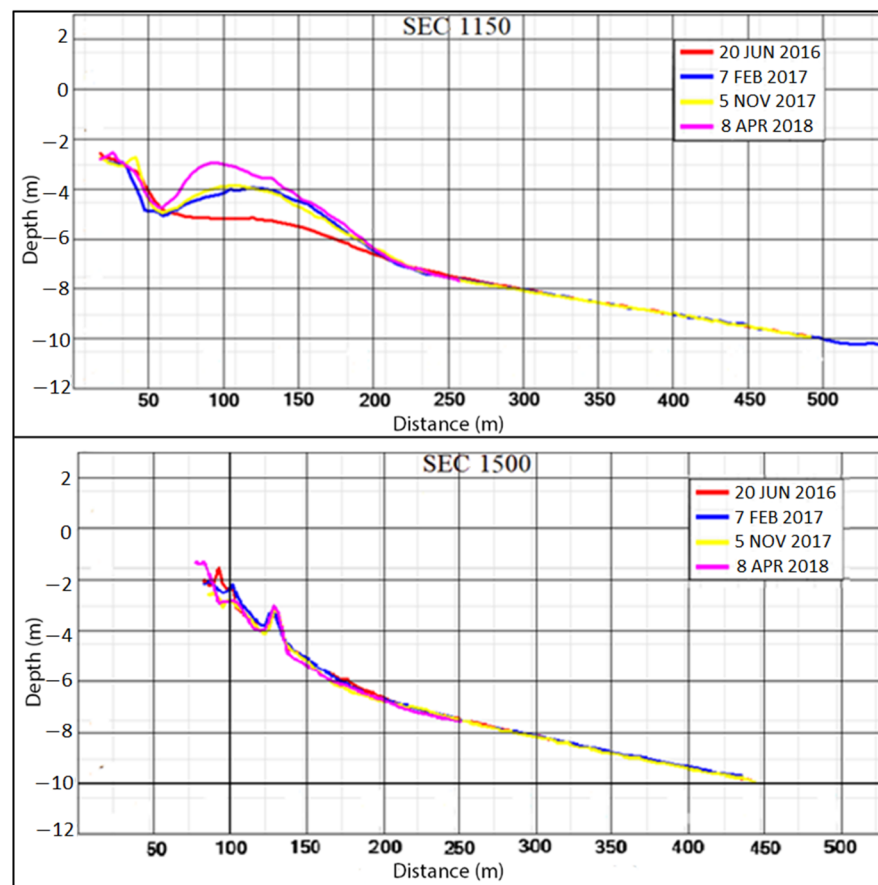
Figure 11. Sequential profile changes recorded for the Sandıktaş HL.
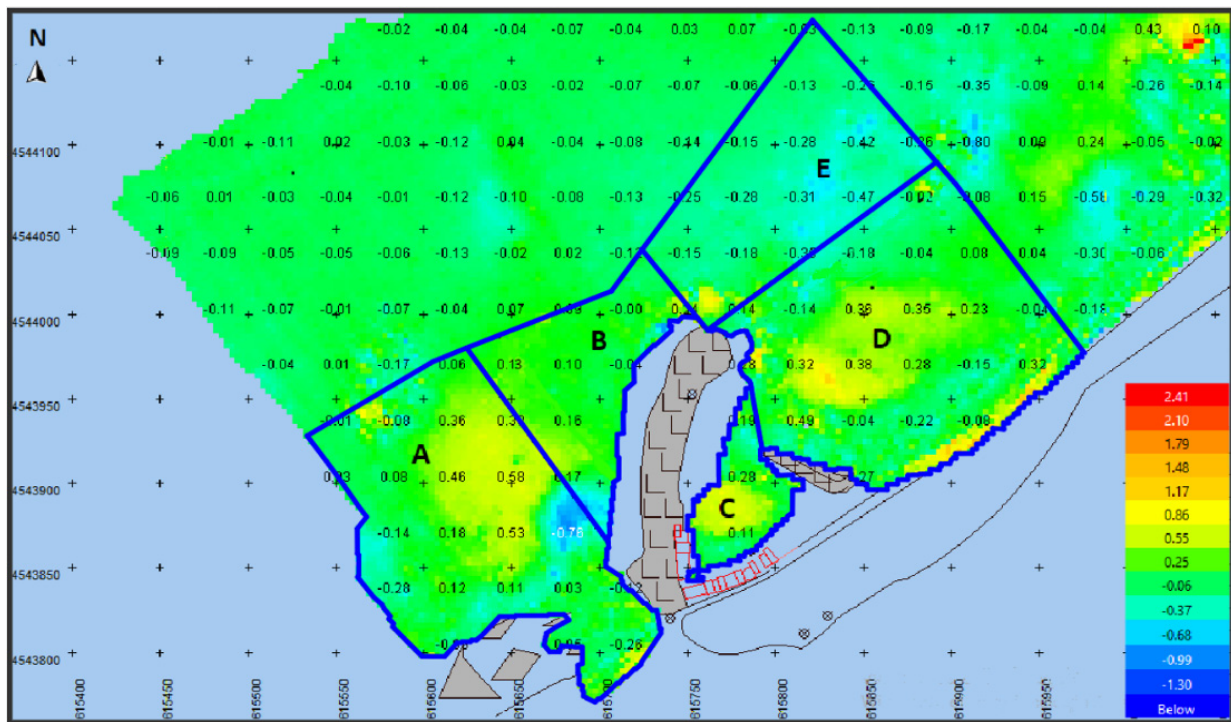
Figure 12. The determined areas for Sarayköy HL. Regions A, D, B, and E represent the southwest, east, west, and outside of the breakwater, respectively, while region C represents the inside of the harbor (negative value refers to the erosion, while positive value refers to accretion between the second and third surveys).

4.3. Evaluation of Bathymetric Changes in the Harbor Launches

In this section, we present bathymetry difference maps that show the seabed changes between two bathymetries in any survey period for every harbor launch of interest. After that, the polygon area, volume difference, and mean vertical variation were determined for each sub-region in each study area. The deposition/erosion amounts/percentages for each sub-region were computed and discussed, taking into account the mean water depths in the sub-regions, wave roses, the dominant wave direction, and wave conditions.

4.3.1. Sandıktaş Harbor Launch

Bathymetry difference maps were created for the Sandıktaş harbor launch. The depth-based differences between the second and third surveys are shown in Figure 13. The polygon areas, volume differences, and average vertical changes obtained from the bathymetry difference maps are given in Table 11. Thus, deposition/erosion percentages were determined (Table 11) and are shown graphically (Figure 14). The volumes were calculated for the first three surveys in region C as -8085 m^3, -5764 m^3, and -390 m^3, respectively. By taking the first measurement as a reference, the ratio of the difference between the first and second measurement values to those of the first measurement iteration was found. According to this ratio, 28.7% of deposition occurred. Likewise, based on the ratio of the difference between the first and third measurement values to those of the first measurement iteration, 95.2% of deposition occurred.

In the Sandıktaş harbor launch area, erosion only appeared in region A; however, deposition occurred in regions B, C, D, and E. It was clearly observed that the direction of sediment transport was from west to east, due to the dominant wave direction (please see Figure 15). While there was an average of 0.04 m^3/m^2 of erosion between the first and second surveys in region A, an average of 0.15 m^3/m^2 of erosion was observed between the first and third surveys. It was seen that the average water depth increased in comparison with the initial position (4.99 m) in subsequent measurements (please see

Table 12). While there was 0.5% of erosion between the second and the third surveys in terms of the deposition/erosion percentage, 2.85% erosion was observed between the first and the third surveys. Region B can be characterized as the transition area. Between the first and the second surveys, an average of 0.12 m^3/m^2 of deposition was observed, and this amount remained constant (Table 11), while the average water depths were 5.63 m, 5.50 m, and 5.53 m, respectively (Table 12). Therefore, seabed changes in the region were not characterized as being stationary.
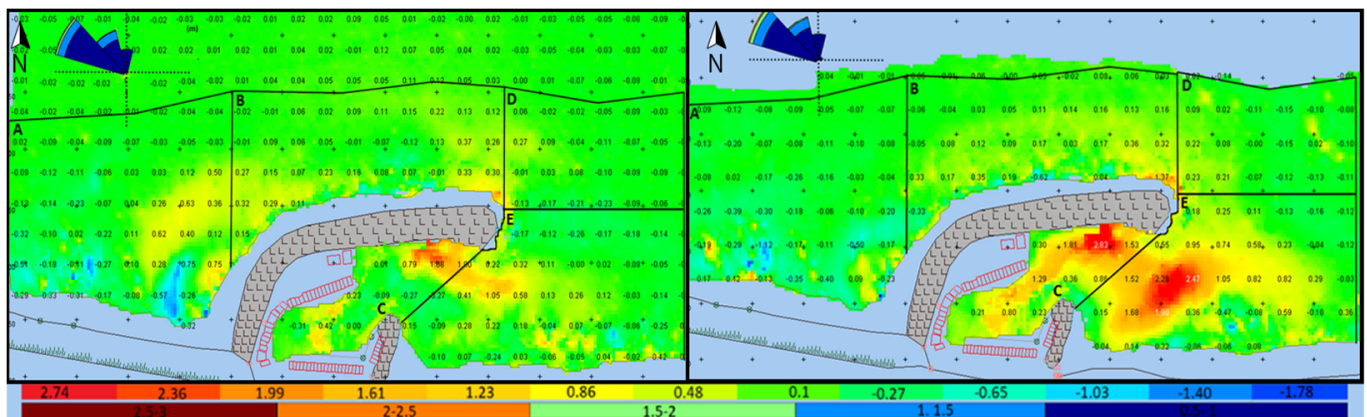
Figure 13. Bathymetry difference maps of the Sandıktaş harbor launch. **Left** image: second measurement–first measurement (5 November 2017–7 February 2017—9 months). **Right** image: third measurement–first measurement (8 April 2018–7 February 2017—14 months). Regions C, A, and D represent the basin, updrift, and downdrift of the harbor launch, respectively, while region B and E represent the upper part and eastward of the breakwater, respectively. (negative value refers to the erosion, while positive value refers to accretion between the surveys).

Table 11. Sandıktaş HL: areas, volume differences, and the average vertical changes of the sub-regions.

Difference of Period	Areas	Polygon Area, m^2	Volume Difference, m^3	Mean Vertical Variation, m^3/m^2
2. Survey−1. Survey (n_2−n_1)	Part A	37,291	−1498	−0.04
	Part B	27,000	3199	0.12
	Part C	9648	3021	0.31
	Part D	16,483	−139	−0.01
	Part E	31,873	2027	0.06
3. Survey−2. Survey (n_3−n_2)	Part A	37,581	−4097	−0.11
	Part B	27,115	−127	0.00
	Part C	10,653	5748	0.54
	Part D	16,281	181	0.01
	Part E	32,682	14,038	0.43
3. Survey−1. Survey (n_3−n_1)	Part A	37,372	−5617	−0.15
	Part B	27,419	3222	0.12
	Part C	9871	8939	0.91
	Part D	16,281	69	0.00
	Part E	32,075	15,971	0.50
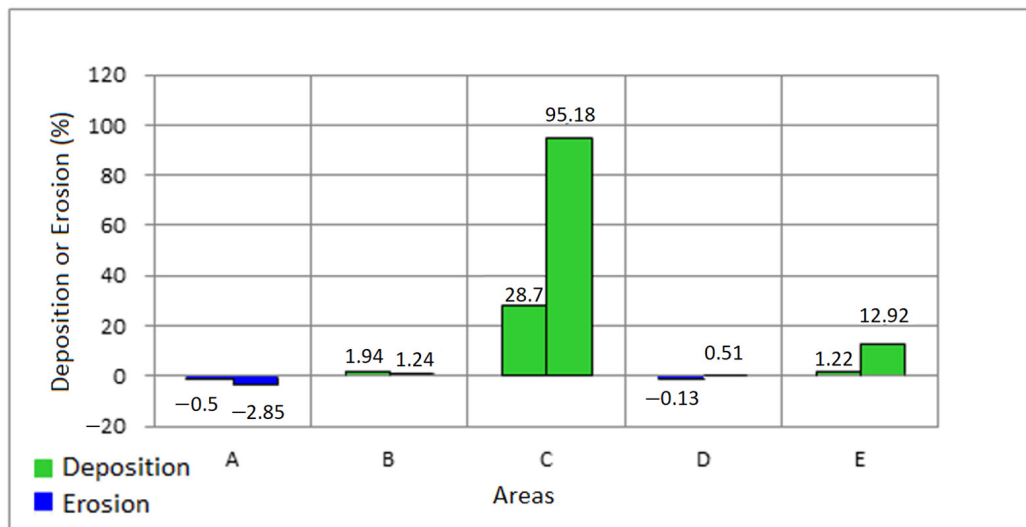
Figure 14. Percentages of deposition or erosion at the Sandıktaş HL. Regions C, A, and D represent the basin, updrift, and downdrift of the harbor launch, respectively, while region B and E represent the upper part and eastward of the breakwater, respectively.
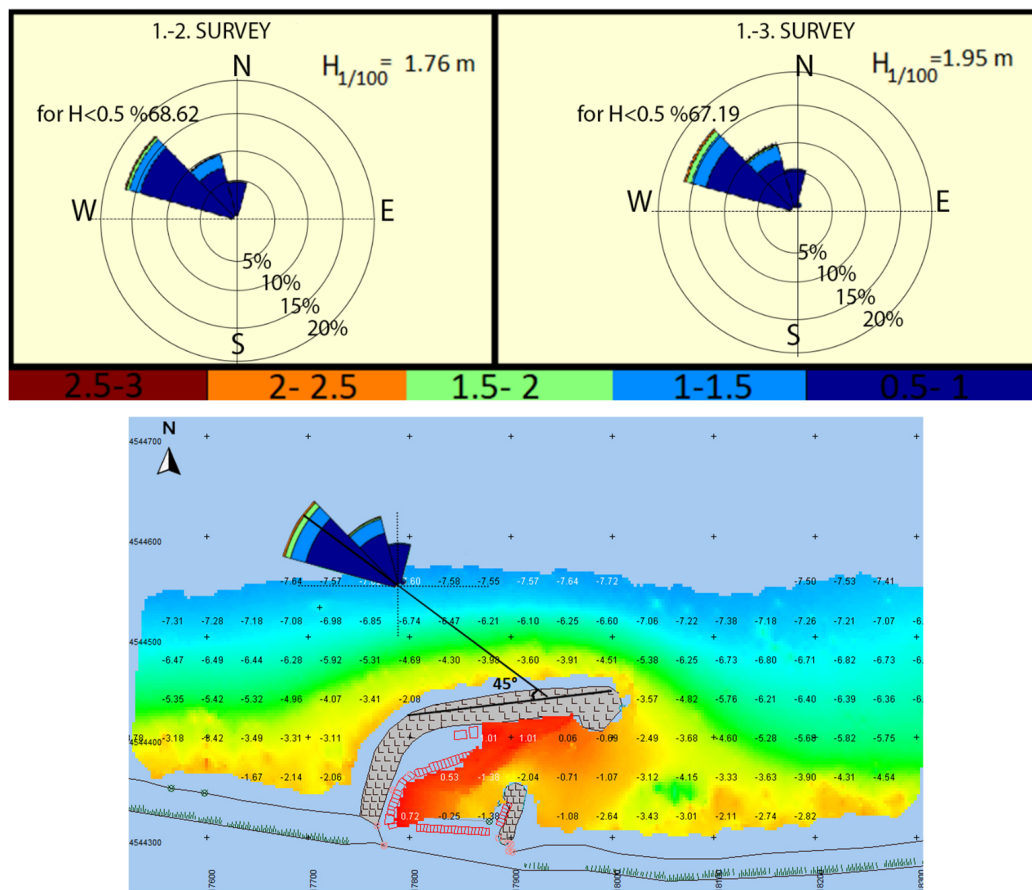
Figure 15. Wave roses formed according to the various time periods for the Sandıktaş HL (**upper images**) and the angle made by the second part of the main breakwater at Sandıktaş with the dominant wave direction (**lower image**). (negative value refers to the depth below the mean sea level).

Table 12. Mean water depths according to the sub-regions for the Sandıktaş HL.

Sandıktaş HL	Mean Water Depths (m)				
	A	**B**	**C**	**D**	**E**
1. Survey—7 February 2017	4.99	5.63	0.90	6.82	3.86
2. Survey—5 November 2017	5.05	5.50	0.65	6.83	3.79
3. Survey—8 April 2018	5.14	5.53	0.04	6.82	3.35

Regions C and E represent the entrance and downstream side of the breakwater, respectively. Significant deposition was observed in both regions. For the second survey, it was seen that the average water depth in region C decreased from 0.90 m to 0.65 m (Table 12). In region E, the average water level decreased to 3.79 m, decreasing by 0.07 m in the second survey. The average depth of region E decreased to 3.35 m by the third survey. Moreover, region C reached an average of 0.04 m in depth, decreasing by 0.61 m in the third survey. The increment of the average layer thickness was 0.31 m^3/m^2 (28.7% deposition/erosion ratio) between the first and second surveys, while the value was 0.91 m^3/m^2 (95.18% deposition/erosion ratio) between the first and third surveys. One of the most important factors causing this interaction is diffraction. Upon reaching the main breakwater, the waves turn toward the inside of the breakwater and continue their movement at a reduced speed, which causes the material they carry to be transported into the inlet and the harbor basin and to settle there. In order to reach this conclusion, wave roses were constructed for different time periods using the wave hindcast data from the station considered within the study region; these are shown in Figure 15 for the Sandıktaş HL. This analysis also shows that the second part of the Sandıktaş HL's main breakwater formed an angle of approximately 45° with the offshore–dominant wave direction. In addition, the height, period, and direction variations of the waves with respect to the time intervals are plotted in Figure 15. In regions A and B, since the wave conditions between the third and second surveys were higher than the wave conditions between the first two surveys, those regions have been subjected to scouring. In regions C and E, despite the increase in wave conditions, the amount of deposition increased with the effects of refraction and diffraction.

Another factor that caused excessive accumulation in region E was the natural rocks found in the sea downstream of the harbor launch. These rocks act as a sand trap by preventing sediment transportation along the coast and causing the material to be retained in that area. This trapped material is transported and accumulated inside the breakwater by small waves coming from the north–northeast direction. The height of the incoming waves for the time interval of the first to the third surveys was higher than for the time interval of the first to the second surveys for $H_{1/100}$, the average of the highest 100 waves (Figure 16). As the wave height increased, the capacity for sediment transport also increased. Region D was exposed to both deposition and erosion at the same time; however, the seabed changes remained in balance. It was observed that the changes in the average layer thickness and the average water depths remained fixed in each survey.

4.3.2. Yanıktaş Harbor Launch

Yanıktaş HL and its vicinity were divided into regions A, B, C, and D. Figure 17 shows the elevation differences between the surveys. The polygon areas, volume differences, and average vertical changes on the bathymetry difference maps are given in Table 13. Based on the bathymetry maps, average water depth and volume values were obtained for each sub-region by taking a reference survey with regard to the bed elevation. Deposition/erosion percentages were obtained by dividing the differences between these volume values (Figure 18). It was observed that there was no overfilling or erosion in Yanıktaş HL, which means that there were no marked changes to the seabed. Region A represents the upstream region of the breakwater. As a result of the second survey, it was observed that an average of 0.16 m^3/m^2 of erosion occurred in the sub-region. After the second survey, deposits in the area had slightly accumulated, and there was 0.14 m^3/m^2 of erosion

between the first and third surveys. After the first survey, the deposition material was transported eastward and erosion occurred in the sub-region, then the material returned to the sub-region from the west and accumulated to a small degree (Table 13). The average water depth value was 5.15 m in the first survey, but this value increased to 5.31 m in the subsequent measurement iteration, and then remained stable, with a very small decrease of 0.02 m.
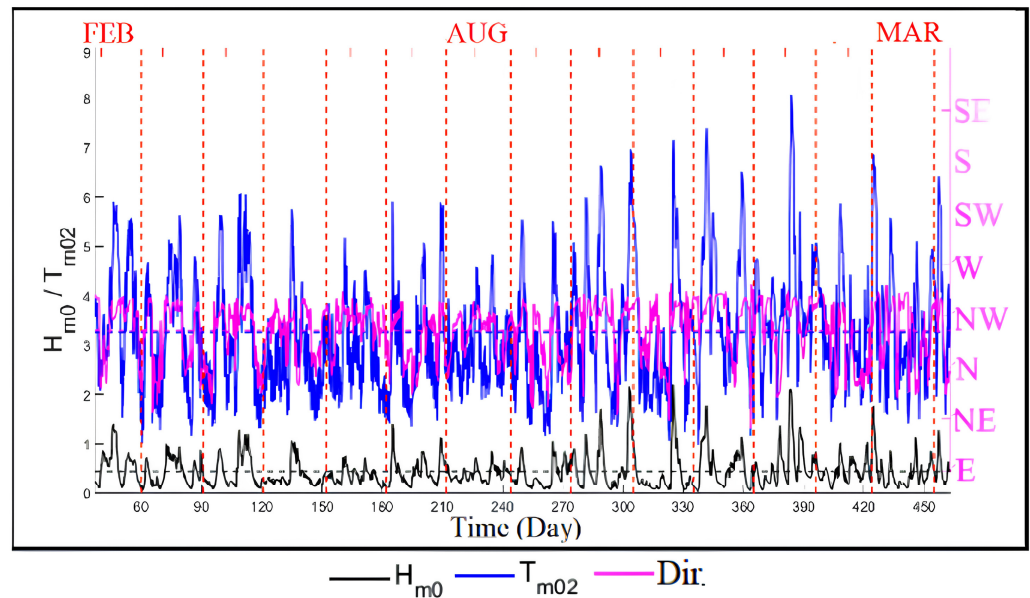
Figure 16. The height, period, and direction variations of the waves between 7 February 2017 and 8 April 2018 (first survey–third survey) at the offshore location of Sandıktaş HL.
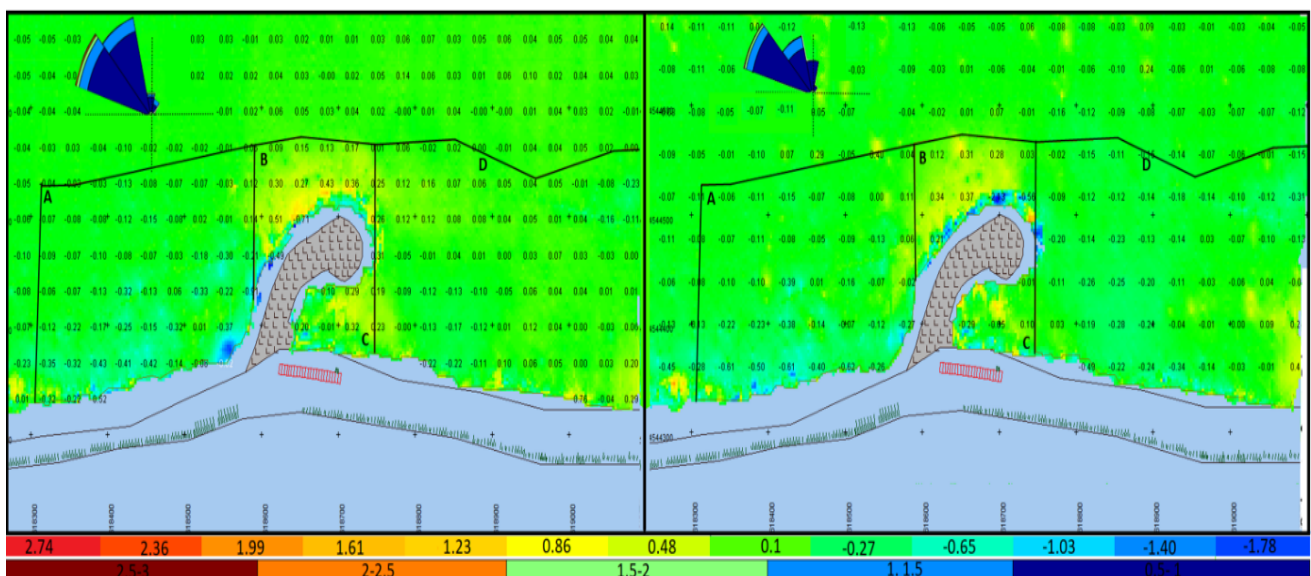
Figure 17. Yanıktaş harbor launch bathymetry difference map. The **left** image shows the differences between the second and first surveys (7 February 2017–20 June 2016—7.5-month period). The **right** image shows differences between the third and the first surveys (5 November 2017–20 June 2016—16.5-month period). Regions C, A, and D represent the basin, updrift, and downdrift of the harbor launch, respectively, while region B represents the upper part of the breakwater (negative value refers to the erosion, while positive value refers to accretion between the surveys).

Table 13. Yanıktaş HL areas, volume differences, and the average vertical changes of the sub-regions.

Difference of Period	Areas	Polygon Area, m^2	Volume Difference, m^3	Mean Vertical Variation, m^3/m^2
2. Survey–1. Survey (y_2–y_1)	Part A	53,860	−8368	−0.16
	Part B	12,555	2477	0.20
	Part C	6040	444	0.07
	Part D	72,829	1004	0.01
3. Survey–2. Survey (y_3–y_2)	Part A	54,263	921	0.02
	Part B	12,743	−11.09	−0.09
	Part C	6337	−493	−0.08
	Part D	72,829	−9134	−0.13
3. Survey–1. Survey (y_3–y_1)	Part A	53,902	−7790	−0.14
	Part B	12,743	1331	0.10
	Part C	6443	14.5	0.00
	Part D	72,829	−8135	−0.11
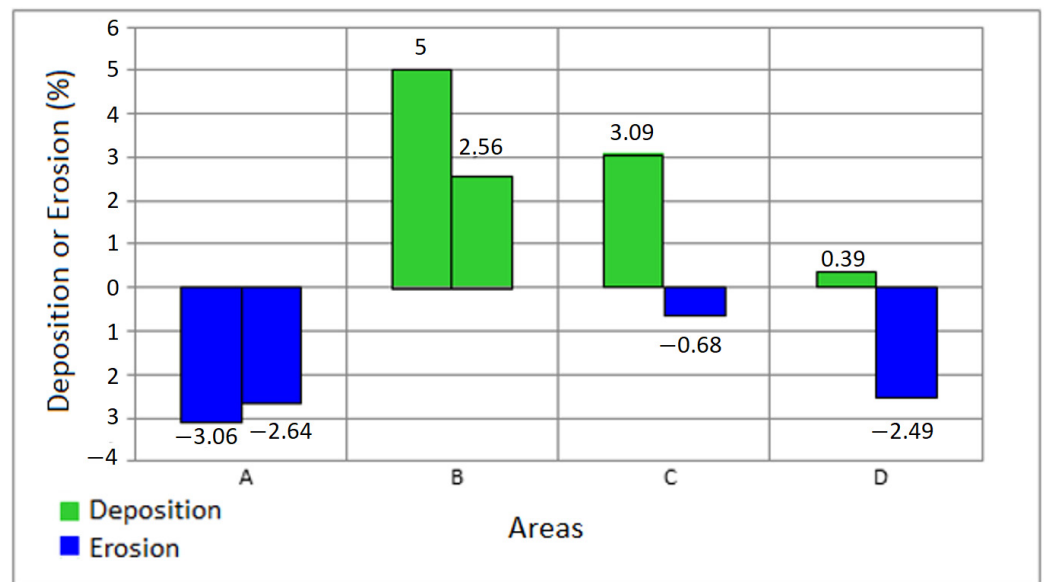
Figure 18. Percentages of deposition or erosion at the Yanıktaş HL. Regions C, A, and D represent the basin, updrift, and downdrift of the harbor launch, respectively, while region B represents the upper part of the breakwater.

In region B, while there was an average accumulation of 0.20 m^3/m^2 between the first and second surveys, this value decreased to 0.10 m^3/m^2 between the first and third surveys (Table 13). There was 5% of deposition between the first and second surveys, whereas this value was halved between the first and third surveys (Figure 18). The average water depth values were 5.13 m, 5.01 m, and 5.04 m at the first, second, and third surveys, respectively (Table 14). Region C represents the basin of the breakwater. The material coming from the west continued to move in the same way, in the direction of net transport, without entering the breakwater. There was very little change in the basin of the breakwater. The average water depths were 2.48 m at the end of the first survey and 2.41 m and 2.50 m in the subsequent surveys, respectively. Seabed changes in the region can be characterized as being stationary. The increment of the dominant wave heights did not affect the shoaling in the breakwater at Yanıktaş HL. Region D was stable between the first two surveys and an average of 0.11 m^3/m^2 of erosion was observed between the first and third surveys. The average water depth values were 4.39 m, 4.38 m, and 4.51 m at the first, second, and third surveys, respectively (Table 14). Figure 19 shows that the second part of the main breakwater in the Yanıktaş HL formed an angle of approximately 75° with the offshore

dominant wave direction. The height of the incoming waves ($H_{1/100}$) in the period between the first and third surveys was higher than the height of the incoming waves in the period between the first and second surveys (Figure 19). As the wave height increased, the longshore transport flow also increased. This was one of the most important reasons why the shoaling effect seen in the breakwater between the first and third surveys was markedly higher than that in the time between the first and second surveys. Likewise, higher wave heights between the first and third surveys caused greater erosion compared with the first two surveys in Region A. The $H_{1/100}$ values and the relative wave roses are shown in Figure 19. The height, period, and direction graphs of the waves are shown in Figure 20. Compared to the angle (approximately 45°) for Sandıktaş harbor, the waves reached the harbor area at an angle closer to the perpendicular (approximately 75°), and the areas were less subject to shoaling and refraction effects, resulting in a low level of accumulation/erosion in and around the harbor basin.

Table 14. Mean water depths, shown by sub-regions, for the Yanıktaş HL.

Yanıktaş HL	Mean Water Depths (m)			
	A	B	C	D
1. Survey—20 June 2016	5.15	5.13	2.48	4.39
2. Survey—7 February 2017	5.31	5.01	2.41	4.38
3. Survey—5 November 2017	5.29	5.04	2.50	4.51
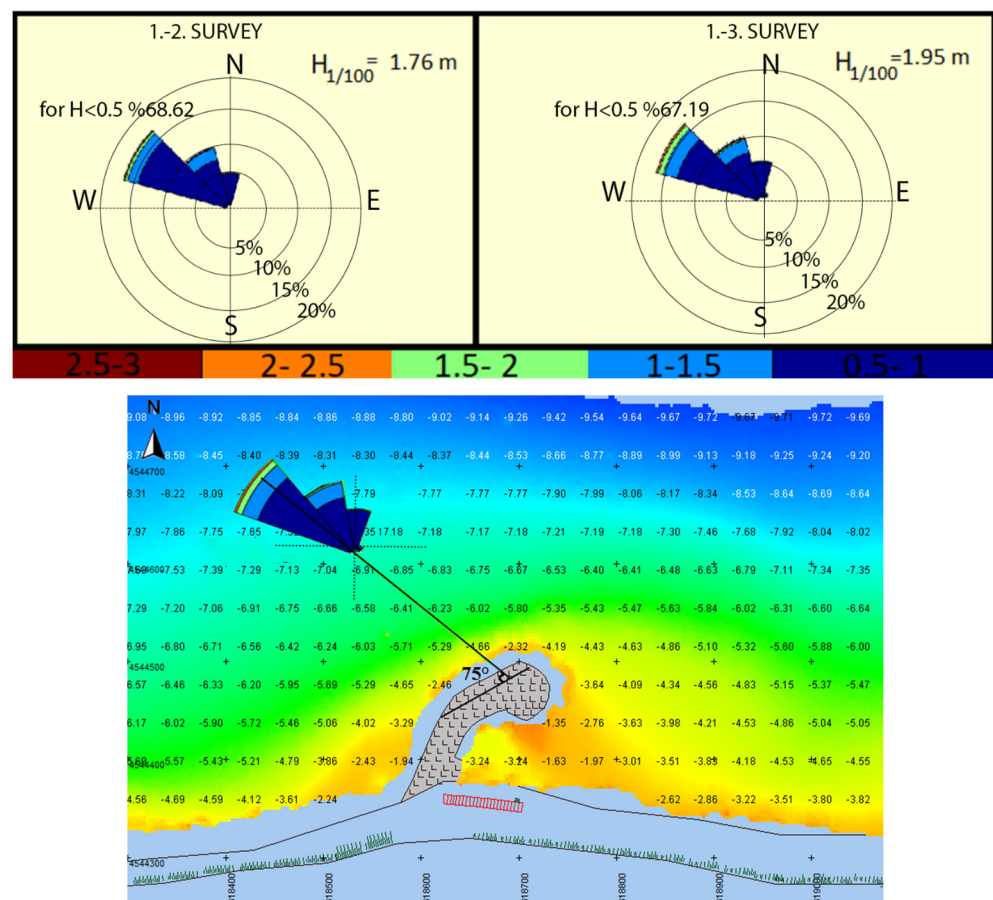
Figure 19. Wave roses formed according to the various time periods for the Yanıktaş HL (**upper images**) and the angle made by the second part of the main breakwater at Yanıktaş HL, along with the dominant wave direction (**lower image**) (negative value refers to the depth below the mean sea level).
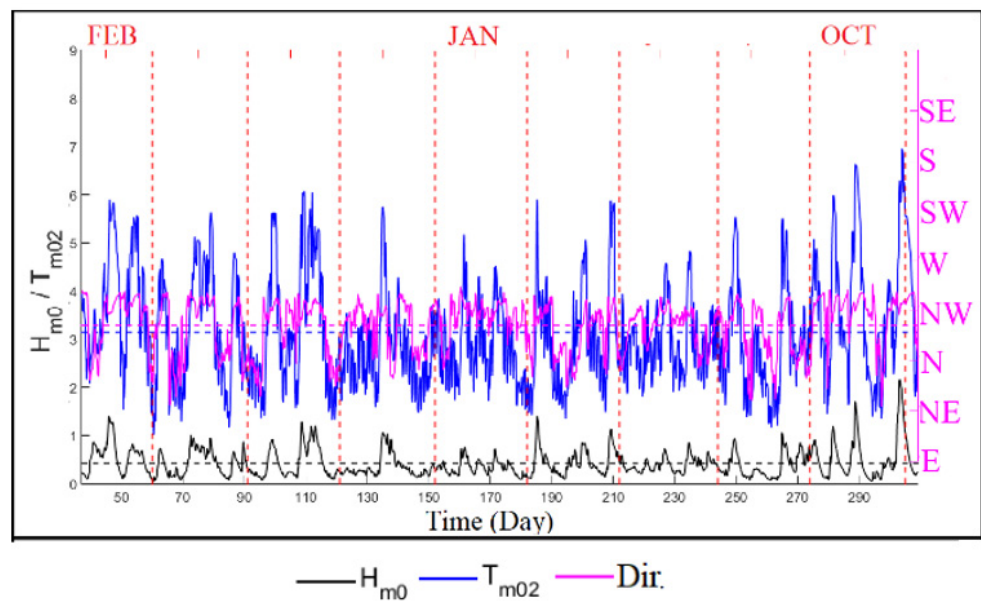
Figure 20. The height, period, and direction variations of the waves between 7 February 2017 and 5 November 2017 (between the second survey and the third survey) at the offshore location of the Yanıktaş harbor launch.

4.3.3. Sarayköy Harbor Launch

Sarayköy HL and its vicinity were divided into five sub-regions, which were designated as A, B, C, D, and E. The bathymetric difference maps are shown in Figure 21. Based on the bathymetry maps, the average water depths and volume differences were calculated for each region by taking as a reference the elevation to the seabed surface (Table 15) (Figure 22).
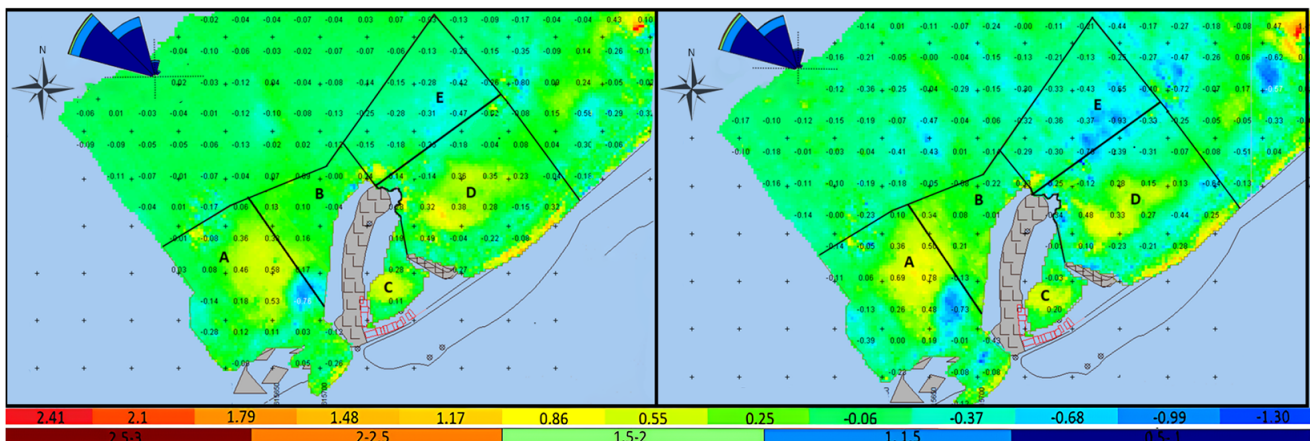
Figure 21. Sarayköy harbor launch bathymetric difference maps. The **left** image shows the differences between the second and the first surveys (29 April 2017–2 June 2016—11 months). The **right** image shows the differences between the third and the first surveys (4 November 2017–2 June 2016—17 months). Regions A, D, B, and E represent the southwest, east, west, and outside of the breakwater, respectively, while region C represents the inside of the harbor (negative value refers to the erosion, while positive value refers to accretion between the surveys).

Table 15. Sarayköy HL areas, volume differences, and the average vertical changes of the sub-regions.

Difference of Period	Areas	Polygon Area, m^2	Volume Difference, m^3	Mean Vertical Variation, m^3/m^2
2. Survey–1. Survey (s_2-s_1)	Part A	23,540	2173	0.09
	Part B	5827	459	0.08
	Part C	3301	610	0.18
	Part D	20,935	2917	0.14
	Part E	16,158	−3384	−0.21
3. Survey−2. Survey (s_3-s_2)	Part A	25,842	−943	−0.04
	Part B	6230	21	0
	Part C	3565	−90	−0.03
	Part D	21,131	−3331	−0.16
	Part E	16,241	−2724	−0.17
3. Survey−1. Survey (s_3-s_1)	Part A	23,759.5	1255	0.05
	Part B	5822	440	0.08
	Part C	3301	539	0.17
	Part D	20,935	−407	−0.02
	Part E	16,094	−6070	−0.38
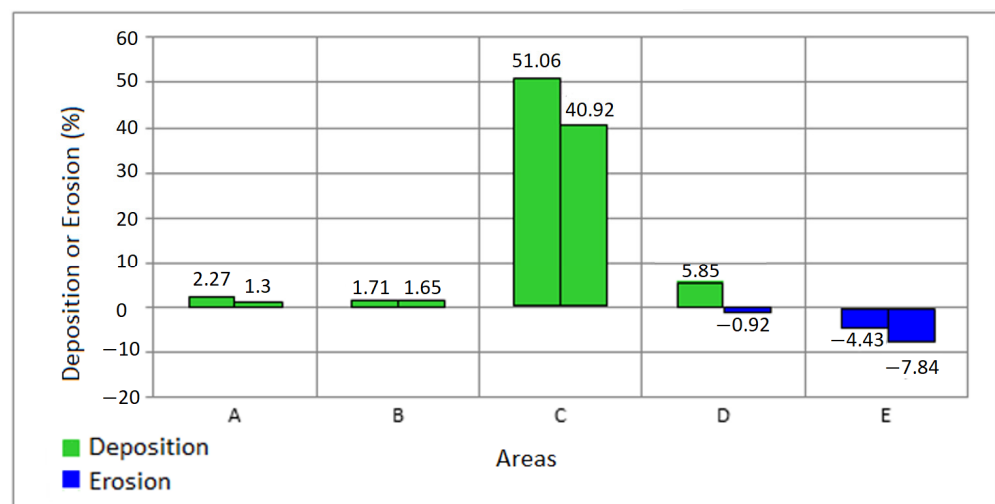
Figure 22. Percentages of deposition or erosion at the Sarayköy HL. Regions A, D, B, and E represent the southwest, east, west, and outside of the breakwater, respectively, while region C represents the inside of the harbor.

Sediment accumulated in regions A, B, C, and D (especially in region C), whereas erosion occurred in region E. After the second survey, the average depths of regions A, B, and C almost did not change, while erosion occurred in regions D and E. Region C represents the basin of the breakwater. There was an average of 0.18 m^3/m^2 of deposition between the first and second surveys; also, an average of 0.17 m^3/m^2 of deposition was observed between the first and the third surveys (Table 15). After the second survey, the water depth decreased from 0.36 m to 0.18 m, then the average water depth value increased to 0.22 m, with an increment of 0.04 m (Table 16). After the second survey, updrift transport continued; therefore, the region remained stable. There were no remarkable differences between the heights of the incoming waves among the surveys, according to the wave analysis (H$_{1/100}$). However, waves coming from a northerly direction in the period between the first and the second surveys were higher than those in the period between the first and the third surveys (Figure 23). This was a factor affecting the disparity of shoaling in the basin of the breakwater between the first two surveys. The average sediment grain diameter of the basin and entrance of the breakwater were coarser than those upstream

and downstream of the breakwater in the Saraýköy HL. This may be caused by the type of material coming from the stream just downstream of the secondary breakwater. It was determined that the second part of the main breakwater of the Saraýköy HL formed an angle of approximately 95° with the offshore dominant wave direction (Figure 23). Wave roses with respect to the time intervals are shown in Figure 23. The height, period, and direction graphs of the waves are shown in Figure 24. In Saraýköy harbor, similar to the situation in Yanıktaş harbor, a low level of erosion/accumulation occurred in other regions except for region C, with the waves reaching the harbor area at an angle perpendicular to the shore. Due to the long length of the main breakwater of Saraýköy harbor, intensely diffracted waves caused a high level of accumulation in region C.

Table 16. Mean water depths, shown by sub-regions, for the Saraýköy HL.

Saraýköy HL	Mean Water Depths (m)				
	A	**B**	**C**	**D**	**E**
1. Survey—2 June 2016	3.82	4.37	0.36	2.36	4.94
2. Survey—29 April 2017	3.73	4.29	0.18	2.22	5.14
3. Survey—4 November 2017	3.76	4.29	0.22	2.38	5.30
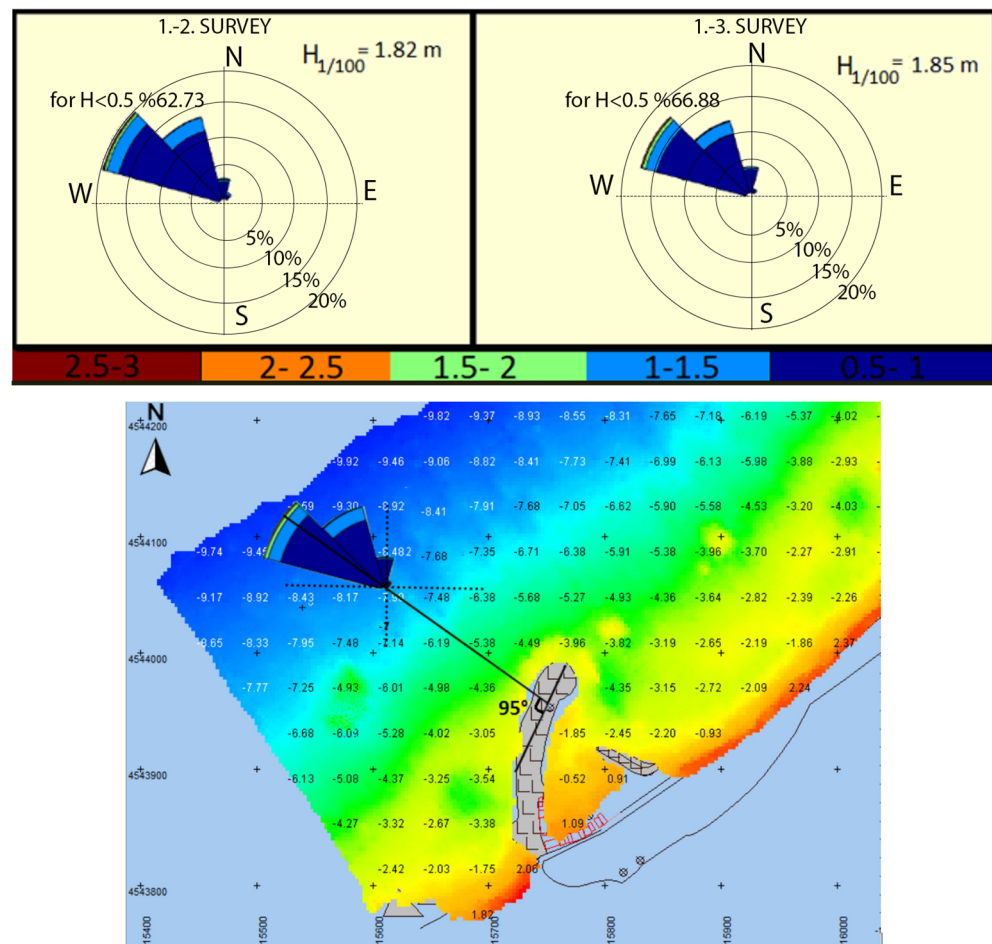
Figure 23. Wave roses, formed according to the various time periods, for the Saraýköy HL (**upper images**), and the angle made by the second part of the main breakwater at the Saraýköy HL with the dominant wave direction (**lower image**) (negative value refers to the depth below the mean sea level, while positive value refers to that above the mean sea level).
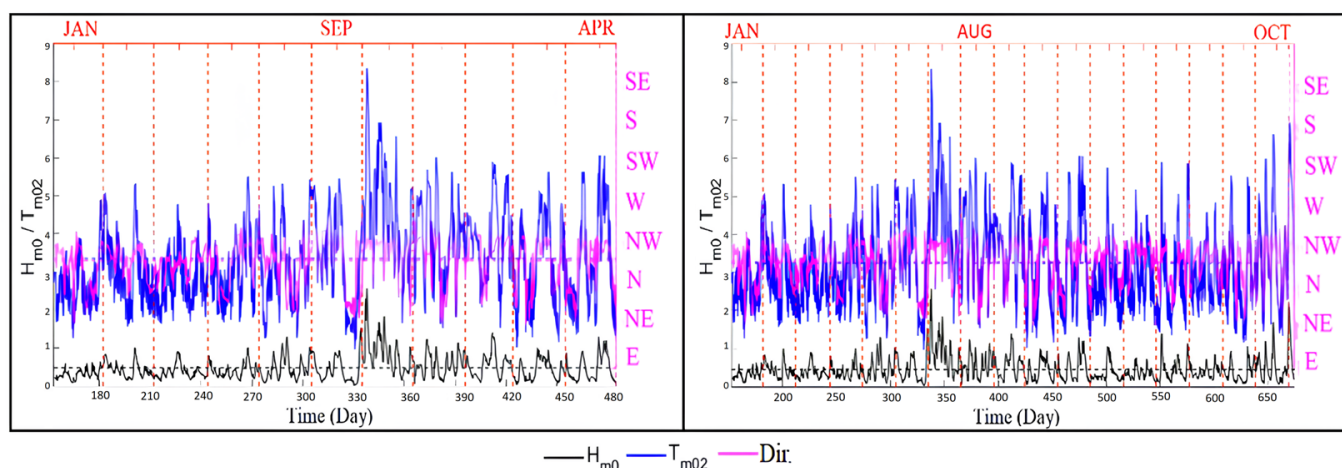
Figure 24. Sarayköy HL: wave height, period, and direction graphics. The **left** image is for the period between 2 June 2016 and 29 April 2017 (from the first to the second surveys). The **right** image is for the period between 2 June 2016 and 4 November 2017 (from the first to the third surveys).

5. Conclusions

The shoaling process was examined in the context of three harbor launches in Rize province in the Eastern Black Sea region. A detailed field study was conducted for the three study areas. Shoaling dynamics and sediment movement in and around the harbors and the effect of waves were analyzed.

The conclusions obtained can be summarized as follows:

- Although Sandıktaş has the longest breakwater length compared to the other harbors, approximately 13,200 m^3 of accumulation occurred inside the breakwater and the entrance of the harbor launch annually. Accumulation of 1100 m^3 and 270 m^3 was observed at the same location for Sarayköy and Yanıktaş, respectively.
- No shoaling effect was observed in the Yanıktaş HL, while a serious shoaling problem was found in the Sandıktaş harbor launch due to the location of the harbor launch, the positioning of the breakwater, and the angle between the main breakwater and the dominant wave direction.
- The sediment transport rate was negligibly low at depths greater than −7 m for all study areas.
- The angle formed by the second part of the main breakwater with the direction of the dominant wave is one of the most important parameters.
- The location of the harbor launch and the positioning of the breakwater are very important. The construction of a longer breakwater is not the only solution to blocking sedimentation due to shoaling.
- The direction of coastal sediment transport was from west to east.
- An additional extension to the main breakwater in Sandıktaş was not sufficiently effective for blocking sedimentation due to shoaling.

The implementation of reliable periodic monitoring studies can significantly contribute to future projects in the area, reduce potential shoaling problems, and ensure the long-term sustainability of the fishing industry in the region.

References

1. Tourlioti, P.N.; Portman, M.E.; Tzoraki, O.; Pantelakis, I. Interacting with the coast: Residents' knowledge and perceptions about coastal erosion (Mytilene, Lesvos Island, Greece). *Ocean Coast. Manag.* **2021**, *210*, 105705. [CrossRef]
2. Cooper, J.A.G.; McKenna, J. Social justice in coastal erosion management: The temporal and spatial dimensions. *Geoforum* **2008**, *39*, 294–306. [CrossRef]
3. Petrakis, S.; Alexandrakis, G.; Poulos, S. Recent and future trends of beach zone evolution in relation to its physical characteristics: The case of the Almiros bay (Island of Crete, south Aegean sea). *Glob. Nest J.* **2014**, *16*, 104–113. [CrossRef]
4. Huang, Y.; Jin, P. Impact of human interventions on coastal and marine geological hazards: A review. *Bull. Eng. Geol. Environ.* **2018**, *77*, 1081–1090. [CrossRef]
5. Mentaschi, L.; Vousdoukas, M.I.; Pekel, J.F.; Voukouvalas, E.; Feyen, L. Global long-term observations of coastal erosion and accretion. *Sci. Rep.* **2018**, *8*, 12876. [CrossRef]
6. Neelamani, S. Coastal erosion and accretion in Kuwait–Problems and management strategies. *Ocean Coast. Manag.* **2017**, *156*, 76–91. [CrossRef]
7. Walker, J.R.; Williams, P.J.; Dunham, J.W. *Santa Cruz Harbor Shoaling Study. Santa Cruz Harbor, California*; Reports Prepared for the San Francisco District, US Army Corps of Engineers; US Army Corps of Engineers: Washington, DC, USA, 1978.
8. Dayananda, H.V.; Gerritsen, F. Sedimentation studies on a small harbor on a coast of high littoral drift. In Proceedings of the International Conference on Coastal and Port Engineering in Developing Countries, Colombo, Sri Lanka, 20–26 March 1983.
9. Parchure, T.M.; Teeter, A.M. *Potential Methods for Reducing Shoaling in Harbors and Navigation Channels*; Technical Report, OCLC: 230741604; US Army Engineer Research and Development Center: Vicksburg, MA, USA, 2003.
10. Parchure, T.M. *Structural Methods to Reduce Navigation Channel Shoaling*; Technical Report, OCLC: 62148217; US Army Engineer Research and Development Center: Vicksburg, MA, USA, 2005.
11. Hughes, S.A.; Hales, L.Z. *Shoaling of Aguadilla Harbor, Puerto Rico*; Technical Report, OCLC: 155845260; US Army Engineer Research and Development Center: Vicksburg, MA, USA, 2007.
12. Bayraktar, E.A. Coastal Effects of T Groins and Shoaling of Fishery Harbors in the Eastern Black Sea Coasts. Master's Thesis, Karadeniz Technical University, Trabzon, Türkiye, 2009.
13. Süme, V.; Yüksek, Ö. Investigation of the shoaling of fishery coastal structures in the Eastern Black Sea coast. *J. Gazi Univ. Fac. Eng. Archit.* **2017**, *33*, 843–852. [CrossRef]
14. Karasu, S.; Marangoz, H.O.; Gülkaya, E.; Akpınar, A.; Ceylan, Y.; Yılmaz, E. Performance based assessment of a small-scale artificially nourished beach. *Ocean Coast. Manag.* **2023**, *224*, 106827. [CrossRef]
15. Gao, J.; Shi, H.; Zang, J.; Liu, Y. Mechanism analysis on the mitigation of harbor resonance by periodic undulating topography. *Ocean Eng.* **2023**, *281*, 114923. [CrossRef]
16. Gao, J.; Ma, X.; Dong, G.; Chen, H.; Liu, Q.; Zang, J. Investigation on the effects of Bragg reflection on harbor oscillations. *Coast. Eng.* **2021**, *170*, 103977. [CrossRef]
17. Duplančić Leder, T.; Baučić, M.; Leder, N.; Gilić, F. Optical satellite-derived bathymetry: An overview and wos and scopus bibliometric analysis. *Remote Sens.* **2023**, *15*, 1294. [CrossRef]
18. Guo, X.; Jin, X.; Jin, S. Shallow Water Bathymetry Mapping from ICESat-2 and Sentinel-2 Based on BP Neural Network Model. *Water* **2022**, *14*, 3862. [CrossRef]
19. Lubac, B.; Burvingt, O.; Nicolae Lerma, A.; Sénéchal, N. Performance and Uncertainty of Satellite-Derived Bathymetry Empirical Approaches in an Energetic Coastal Environment. *Remote Sens.* **2022**, *14*, 2350. [CrossRef]
20. Evagorou, E.; Argyriou, A.; Papadopoulos, N.; Mettas, C.; Alexandrakis, G.; Hadjimitsis, D. Evaluation of Satellite-Derived Bathymetry from High and Medium-Resolution Sensors Using Empirical Methods. *Remote Sens.* **2022**, *14*, 772. [CrossRef]
21. Bergsma, E.W.; Almar, R.; Rolland, A.; Binet, R.; Brodie, K.L.; Bak, A.S. Coastal morphology from space: A showcase of monitoring the topography-bathymetry continuum. *Remote Sens. Environ.* **2021**, *261*, 112469. [CrossRef]
22. Jagalingam, P.; Akshaya, B.J.; Hegde, A.V. Bathymetry mapping using Landsat 8 satellite imagery. *Procedia Eng.* **2015**, *116*, 560–566. [CrossRef]
23. Guo, Y.; Feng, C.; Xu, W.; Liu, Y.; Su, D.; Qi, C.; Dong, Z. Water-land classification for single-wavelength airborne LiDAR bathymetry based on waveform feature statistics and point cloud neighborhood analysis. *Int. J. Appl. Earth Obs. Geoinf.* **2023**, *118*, 103268. [CrossRef]
24. Janowski, L.; Wroblewski, R.; Rucinska, M.; Kubowicz-Grajewska, A.; Tysiac, P. Automatic classification and mapping of the seabed using airborne LiDAR bathymetry. *Eng. Geol.* **2022**, *301*, 106615. [CrossRef]
25. Wang, C.; Li, Q.; Liu, Y.; Wu, G.; Liu, P.; Ding, X. A comparison of waveform processing algorithms for single-wavelength LiDAR bathymetry. *ISPRS J. Photogramm. Remote Sens.* **2015**, *101*, 22–35. [CrossRef]

26. Szafarczyk, A.; Toś, C. The use of green laser in LiDAR bathymetry: State of the art and recent advancements. *Sensors* **2022**, *23*, 292. [CrossRef]

27. Alevizos, E.; Oikonomou, D.; Argyriou, A.V.; Alexakis, D.D. Fusion of drone-Based RGB and multi-spectral imagery for shallow water bathymetry inversion. *Remote Sens.* **2022**, *14*, 1127. [CrossRef]

28. Xuekui, W.; Qingquing, W. Study on sedimentation characteristics of soft clay. In Proceedings of the 3rd International Conference on Energy Resources and Sustainable Development (ICERSD 2020), Harbin, China, 25–27 December 2020. [CrossRef]

29. Kimmoun, O.; Hsu, H.C.; Hoffmann, N.; Chabchoub, A. Experiments on uni-directional and nonlinear wave group shoaling. *Ocean Dyn.* **2021**, *71*, 1105–1112. [CrossRef]

30. Bottin, R.R. *Design Wave and Shoaling Protection, Ventura Harbor, California*; Technical Report, OCLC: 23993027; US Army Engineer Research and Development Center: Vicksburg, MA, USA, 1991.

31. Günbak, A.; Gökçe, K.T.; Güler, I. Sedimentation and erosion problems of Yakakent Fishery Harbor. In Proceedings of the 23rd International Conference on Coastal Engineering, Venice, Italy, 4–9 October 1992.

32. Thompson, E.F.; Diramos, I.P.; Bottin, R.R. *Comparison of Predicted and Measured Shoaling at Morro Bay Harbor Entrance, California*; Technical Report, OCLC: 225248141; US Army Engineer Research and Development Center: Vicksburg, MA, USA, 2002.

33. Güner, H.A.A.; Yüksel, Y.; Çevik, E.Ö. Determination of shoreline evolution: A case study. In Proceedings of the 2011 Conference on Coastal Engineering Practice, San Diego, CA, USA, 21–24 August 2011; World Scientific: Singapore, 2011.

34. Moritz, H.R.; Norton, J.K.; Groth, K.C. *Evaluating Opportunities to Reduce Shoaling within the Federal Navigation Channel at Port Orford: A Relative Comparison of Breakwater Repair Alternatives*; Supplemental Project Report; US Army Engineer Research and Development Center: Vicksburg, MA, USA, 2018.

35. Sharaan, M.; Ibrahim, M.G.; Iskander, M.; Masria, A.; Nadaoka, K. Analysis of sedimentation at the fishing harbor entrance: Case study of El-Burullus, Egypt. *J. Coast. Conserv.* **2018**, *23*, 1143–1156. [CrossRef]

36. Klante, C. *Sediment Transport and Bathymetric Change at Hornafjörður Tidal Inlet: Field Data Analysis and Mathematical Modeling*; TVVR; Lund University: Lund, Sweden, 2018; Volume 18. Available online: https://lup.lub.lu.se/record/5904bc2d-f7d0-4ec4-9 5f7-e6f13377417c (accessed on 20 October 2023).

37. Mojabi, M.; Hejazi, K.; Karimi, M. Numerical investigation of effective harbor geometry parameters on sedimentation inside square harbors. *Int. J. Mar. Sci. Eng.* **2013**, *3*, 57–68.

38. Bottin, R.R.; Mize, M.G. *St. Paul Harbor, St. Paul Island, Alaska Design for Wave and Shoaling Protection*; Technical Report, OCLC: 18736041; US Army Engineer Research and Development Center: Vicksburg, MA, USA, 1988.

39. Özölçer, İ.H.; Kömürcü, M.İ.; Birben, A.R.; Yüksek, Ö.; Karasu, S. Effects of T-shape groin parameters on beach accretion. *Ocean Eng.* **2006**, *33*, 382–403. [CrossRef]

40. Yüksek, Ö. Effects of breakwater parameters on shoaling of fishery harbors. *J. Waterw. Port Coast. Ocean Eng.* **1995**, *121*, 13–22. [CrossRef]

41. Seabergh, W.C.; McCoy, J.W. *Prevention of Shoaling at Little Lake Harbor, Michigian*; Technical Report, OCLC: 870338420; U.S. Army Engineer Waterways Experiment Station: Vicksburg, MS, USA, 1982.

42. Simav, Ö.; Şeker, D.Z.; Tanık, A.; Gazioğlu, C. Determination of risk areas of Turkish coasts with coastal vulnerability indicator. *Map Mag.* **2015**, *153*, 1–8.

43. DLH. *Fishery Coastal Structures Situation and Needs Analysis, 1*; DLH: Ankara, Türkiye, 2011.

44. Karataş, E.; Karataş, A. The importance of fishery production as an income source in Türkiye. *J. Surv. Eng. Fish. Sci.* **2017**, *4*, 38–53.

45. DLH. *Fishery Coastal Structures Situation and Needs Analysis, 2*; DLH: Ankara, Türkiye, 2011.

46. TUSAGA-Active System Working Principle. Available online: https://tkgm.gov.tr/sites/default/files/2020-10/tusaga-aktif_ sistemi.pdf (accessed on 28 June 2020).

47. Alpar, B.; Doğan, E.; Yüce, H.; Altıok, H. Sea level changes along the Turkish coasts of the Black Sea, the Aegean Sea and the Eastern Mediterranean. *Mediterr. Mar. Sci.* **2000**, *1*, 141–156. [CrossRef]

48. Volkov, D.L.; Landerer, F.W. Internal and external forcing of sea level variability in the Black Sea. *Clim. Dyn. J.* **2015**, *45*, 2633–2646. [CrossRef]

49. Defant, A. *Physical Oceanography*; Macmillan: Plymouth, MI, USA, 2007; pp. 1–827.

50. *ASTM 422*; Standard Test Method for Particle-Size Analysis of Soils. ASTM: Philadelphia, PA, USA, 2007.

51. *ASTM 2487*; Standard Practice for Classification of Soils for Engineering Purposes (Unified Soil Classification System). ASTM: Philadelphia, PA, USA, 2006.

52. Booij, N.; Holthuijsen, L.H.; Ris, R.C. A third-generation wave model for coastal regions. Model description and validation. *J. Geophys. Res.* **1999**, *104*, 7649–7666. [CrossRef]

53. Holthuijsen, L.H.; Booij, N.; Ris, R.C. A spectral wave model for the coastal zone. In Proceedings of the 2nd International Symposium on Ocean Wave Measurement and Analysis, New Orleans, LA, USA, 25–28 July 1993; pp. 630–641.

54. Akpınar, A.; Bingölbali, B.; Van Vledder, G.P. Wind and wave characteristics in the Black Sea based on the SWAN wave model forced with the CFSR winds. *Ocean Eng.* **2016**, *126*, 276–298. [CrossRef]

55. General Bathymetric Chart of the Oceans (GEBCO) Bathymetry Data. 2019. Available online: https://www.gebco.net/data_and_ products/gridded_bathymetry_data (accessed on 20 November 2022).

56. Saha, S.; Moorthi, S.; Wu, X.; Wang, J.; Nadiga, S.; Tripp, P.; Behringer, D.; Hou, Y.T.; Chuang, H.Y.; Iredell, M.; et al. The NCEP climate forecast system version 2. *J. Clim.* **2014**, *27*, 2185–2208. [CrossRef]
57. Komen, G.J.; Cavaleri, L.; Donelan, M.; Hasselmann, K.; Hasselmann, S.; Janssen, P.A.E.M. *Dynamics and Modeling of Ocean Waves*; Cambridge University Press: La Vergne, TN, USA, 1994.
58. Janssen, P.A. Quasi-Linear theory of wind-wave generation applied to wave forecasting. *J. Phys. Oceanogr.* **1991**, *21*, 1631–1642. [CrossRef]
59. Janssen, P.A. Consequences of the effect of surface gravity waves on the mean air flow. In Proceedings of the International Union of Theoretical and Applied Mechanics (IUTAM), Sydney, Australia, 3–5 June 1991.
60. Hasselmann, K.; Raney, R.K.; Plant, W.J.; Alpers, W.; Shuchman, R.A.; Lyzenga, D.R.; Rufenach, C.L.; Tucker, M.J. Theory of synthetic aperture radar ocean imagin: A MARSEN view. *J. Geophys. Res. Oceans* **1985**, *90*, 4659–4686. [CrossRef]
61. Zijlema, M.; Van Vledder, G.P.; Holthuijsen, L.H. Bottom friction and wind drag for wave models. *Coast. Eng.* **2012**, *65*, 19–26. [CrossRef]
62. Battjes, J.A.; Janssen, J.P.F.M. Energy loss and set-up due to breaking of random waves. In Proceedings of the 16th International Conference on Coastal Engineering, Hamburg, Germany, 27 August–3 September 1978.
63. Eldeberky, Y.; Battjes, J.A. Spectral modeling of wave breaking: Application to Boussinesq equations. *J. Geophys. Res. Oceans* **1996**, *101*, 1253–1264. [CrossRef]